SYNTHESIS AND CHARACTERIZATION OF CORE-SHELL NANOPARTICLES FOR PROTON EXCHANGE MEMBRANE FUEL CELLS

by

Kübra AVRUPALI

B.S., Chemistry, Faculty of Engineering, Istanbul University, 2011

Submitted to the Institute for Graduate Studies in
Science and Engineering in partial fulfillment of
the requirements for the degree of
Master of Science

Graduate Program in Chemistry
Bogazici University

2015

Dedicated to my dear family and my love Onur Bilge Pusat

ACKNOWLEDGEMENTS

I would like to thank my thesis supervisor Assist. Prof. Oktay DEMİRCAN for his endless encouragement and support. Throughout the thesis, his positive attitude has been the most encouraging force for me to pursue my thesis with an ambition. I am so grateful for his contribution to my chemistry and experimental knowledge.

I would like to express my thanks to Assoc. Prof. Selmiye ALKAN GÜRSEL for her recommendations.

I wish to extend my thanks to Assist. Prof. Bülent AKGÜN for his careful and constructive review of the final manuscript and attending my defense jury.

I am so glad to work with enthusiastic and hardworking friends. I wish to express my great thanks to Aydın HAŞİMOĞLU for his patience and helpfulness. Also, I would like to thank Belgin CESUR, Ekin POMAY, Begüm NAMLI, Ömercan YILDIRIM, Ayşenur Eslem KISA and Tuğba Muhlise OKYAY for their friendship, support and the best memories. I would like to extend my thanks to Ercan OLGUNSOY for his endless support and friendship. Additionally, I would like to thank Boğaziçi University Track and Field Team and Demircan Group members for their motivation.

My deepest thanks go to my family, my dear father Çetin AVRUPALI, my lovely mother Gülseren AVRUPALI and my precious brother Erdem AVRUPALI for their love and support.

Finally, I wish to express my gratitude to my love Onur Bilge PUSAT for his unfailing love, endless support, patience and encouragement to concentrate on my study.

ABSTRACT

SYNTHESIS AND CHARACTERIZATION OF CORE-SHELL NANOPARTICLES FOR PROTON EXCHANGE MEMBRANE FUEL CELLS

In recent years, low-carbon and non-carbon producing methods are investigated and applied all over the world owing to a more environmentally conscious society. Within these methods, fuel cells show great potential for clean energy production with high efficiency and power density. A fuel cell is an electrochemical energy conversion device which directly converts chemical energy into electrical energy. Proton exchange membrane fuel cells (PEMFC) are preferred due to low operation temperature, rapid start-up, low-weight and longer operating life. Therefore PEMFCs are generally used in automotive and stationary power applications. The membrane is solid polymer electrolyte, which is bonded to catalyzed porous electrodes (anode and cathode) placed on each side. Both anode and cathode are usually composed of a Pt-containing catalyst on conductive carbon. The cost of electrodes is an important barrier to widespread commercialization. The high cost of the electrodes is mostly due to the expensive platinum based catalysts. In this Project, core-shell nanoparticles are used to develop low-cost electrodes. These electrodes replace the expensive platinum ones. Some of transition metals which are nickel, cobalt and copper are used as core and platinum used as a shell. Core-shell nanoparticles are synthesized with borohyride reduction mechanism. In this study Ni-Pt core-shell nanoparticles sub 10 nm are aimed to synthesize. Core-shell nanoparticles are evaluated by using transmission electron microscopy (TEM), cyclic voltammetry (CV), rotating disk electrode (RDE), X-ray diffraction (XRD), X-ray photoelectron spectroscopy (XPS) and performance test.

ÖZET

PROTON ELEKTROLİT MEMBRANLI YAKIT PİLLERİ İÇİN MERKEZ-KABUK NANOPARÇACIK SENTEZİ VE KARAKTERİZASYONU

Son yıllarda, tüm dünyada giderek artan çevresel bilinç ile birlikte düşük karbonlu ve karbon üretimi olmayan metodlar araştırılıp, uygulanmaktadır. Bu metodların içerisinde yakıt pilleri çevre dostu enerji üretimi, yüksek verim ve güç yoğunluğuna sahip olması sebebiyle harika bir potansiyel olarak öngörülmektedir. Yakıt pilleri kimyasal enerjiyi doğrudan elektrik enerjisine dönüştürebilen cihazlardır. Proton elektrolit membranlı yakıt pillerinin tercih edilmesinin sebepleri; düşük sıcaklıkta çalışmaları, hafif olmaları, uzun kullanım ömrüne ve hızlı bir başlangıç hızına sahip olmalarıdır. PEM yakıt pilleri genellikle otomotiv ve jeneratörler gibi sabit güç sistemlerinde kullanılmaktadır. Membran olarak katı polimer elektrolit tabaka kullanılır ve bu tabaka gözenekli katalizör elektrotlara (anot ve katot) bağlı olacak şekilde orta kısımda bulunur. Hem anot hemde katotun yapısında iletken bir karbon üzerinde platin içeren katalizörler bulunur. Elektrotlar platin içerdiklerinden dolayı oldukça maliyetlidir ve bu durum elektrotların yaygın olarak ticarileşmesisinin önünde önemli bir engeldir. Bu projede, merkez-kabuk nanoparçacık modeli düşük maliyetli elektrot üretimi için kullanılacaktır. Merkez-kabuk nanoparçacık özelliğine sahip elektotlar yüksek maliyetli platin elektrotların yerine kullanılacaktır. Merkez-kabuk nanoparçacık modelinde merkezde (iç kısımda) bakır, kobalt ve nikel gibi geçiş metalleri kullanılırken, kabukta (dış kısımda) platin ince bir tabaka halinde düşük miktarda kullanılacaktır. Merkez-kabuk nanoparçacık yönteminde borhidrür indirgeme mekanizması kullanılacaktır. Bu model ile 10 nanometrenin altında merkez-kabuk nanoparçacık sentezi hedeflenmektedir. Merkez-kabuk nanoparçacıkların değerlendirilmesi ise geçirimli electron mikroskobu (TEM), döngüsel voltametri (CV), döner disk elektrot (RDE), X-ışını kırılımı (XRD), X-ışınları fotoelektron spektroskopisi (XPS) ve performans testi yapılarak belirlenecektir.

TABLE OF CONTENTS

LIST OF FIGURES

LIST OF TABLES

1. INTRODUCTION

1.1. Energy Sources

It is a verified fact that energy is the basis of economic development. Nowadays, it is impossible to think a modern civilization without a well-established energy industry and sources. Due to their limited existence, mankind has always searched for new ways to use energy resources more efficiently. There have been a number of reformative changes on the way to use energy during the history, from the original steam engine to internal combustion engines.

Since the twentieth century, fossil fuels are the most common sources of energy in the world. Thermal systems such as internal combustion engines and turbines that employ fossil fuels can be considered as the conventional ways to generate mechanical and electrical energy. However, thermal systems emit heat and carbon dioxide (CO_2) as by-products and these systems are inefficient due to releasing a large amount of waste and by-products into the atmosphere. In addition, atmospheric CO_2 level increases [1].

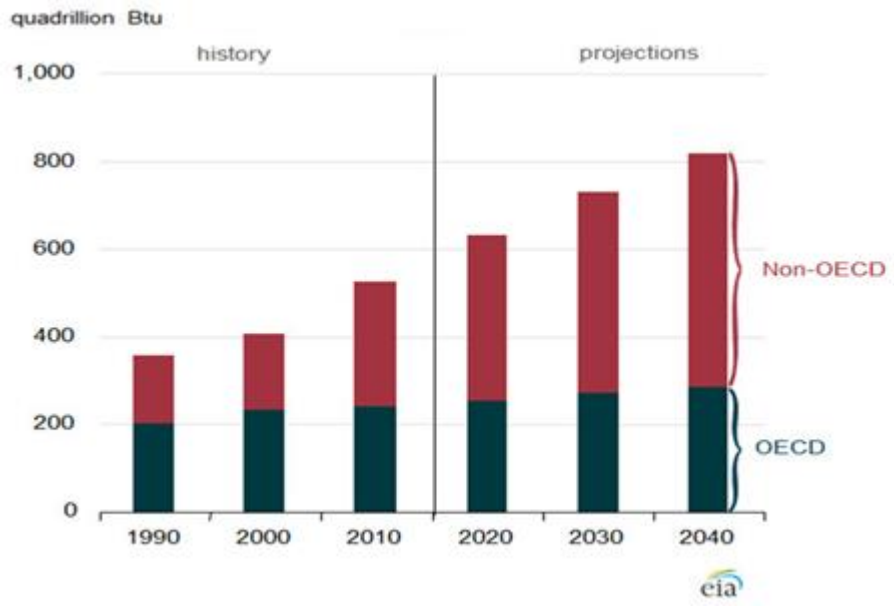

Figure 1.1. World marketed energy consumption, 1990 - 2040.

According to International Energy Outlook 2013 by the Energy Information Administration (EIA) the total world energy use will rise day by day, in 2040 due to economic growth in all countries, an increase of more than 50% over the projection period (Figure 1.1) [2].

International Energy Outlook 2013 assumes that petroleum and coal will continue to be the primary source of fuel and supply to meet the projected increase in energy consumption worldwide. However, the fastest growing sources of world energy are renewables. The renewables share of total energy use rises from 11% in 2010 to 15% in 2040 (Figure 1.2) [2].

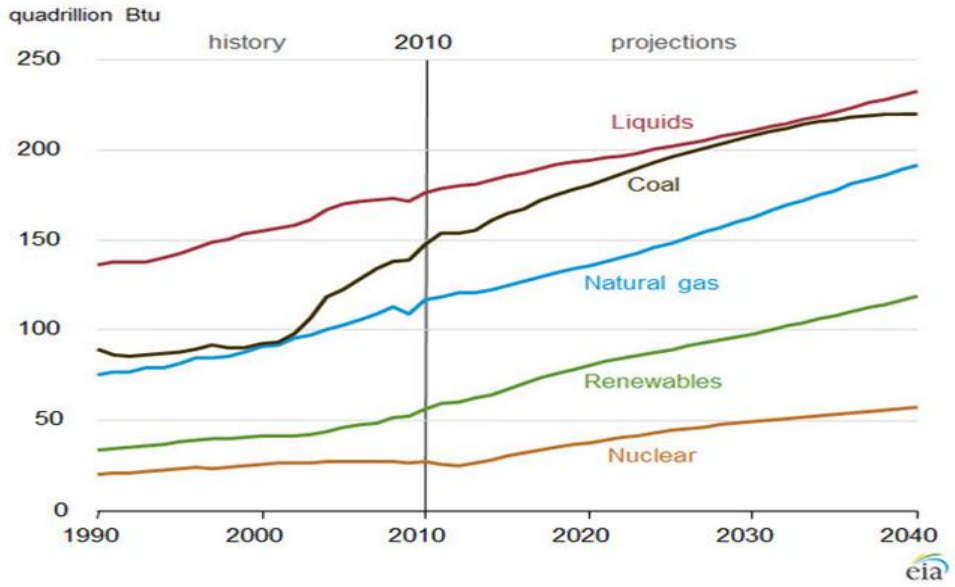

Figure 1.2. World marketed energy use by fuel type, 1990 - 2040.

In many developed economies, increasing energy demand and the environmental concerns due to air pollution and the green house effect of fossil fuels are the primary reasons of the increasing interest shown to renewable alternative energy resources. As the quantity of global reserves of fossil fuels has decreased, the price of oil and natural gas have increased [3]. Hence, those who aim to have a sustainable economic development started to take advantage of the renewable energy that is more cost efficient in the long run. As a result, renewable energy sources are the fastest growing sources of electricity generation in the IEO 2013, at 2.8% per year from 2010 to 2040. There are many forms of

renewable energy such as solar energy, wind power, hydroelectric energy, geothermal power, biomass, hydrogen and fuel cells. Among these alternatives, hydrogen has a life changing opportunity for humans (Figure 1.3).

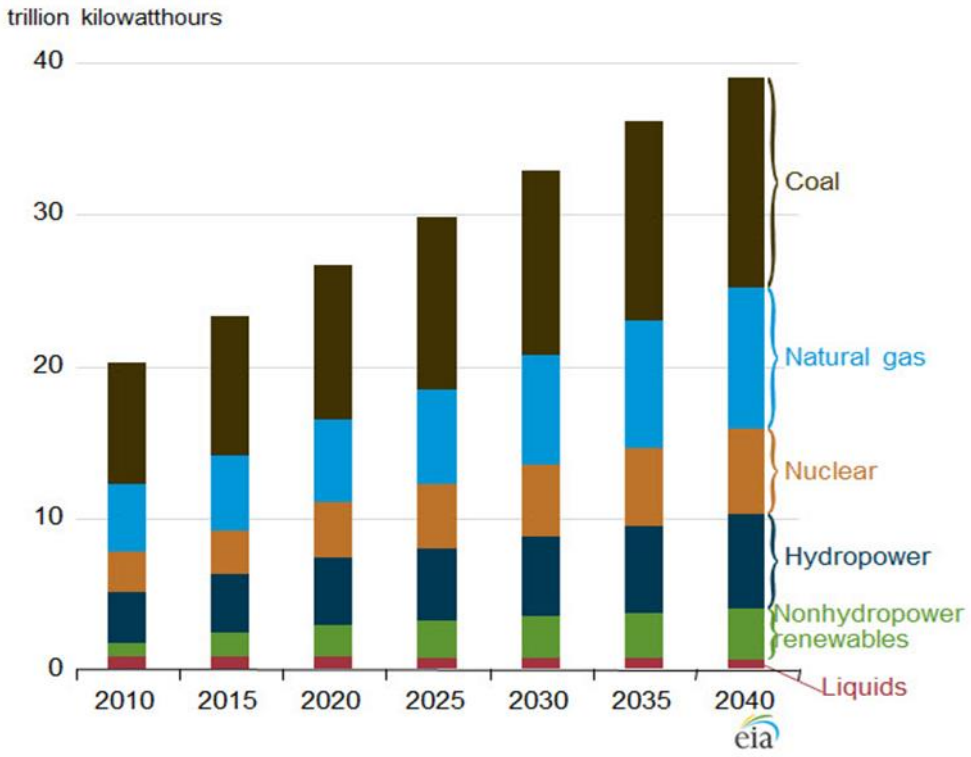

Figure 1.3. World net electricity generation by energy source, 2010 - 2040.

Fuel cells are known as an alternative renewable method of energy generations which are in the hydropower class of renewable energy sources due to using hydrogen as a fuel. The fuel cell does not require recharging in the same way as a battery [4]. It will produce electricity as long as fuel is constantly supplied. The basic design of fuel cell includes two electrodes and an electrolyte. Hydrogen as fuel and oxygen as oxidant flow through each of the electrodes, hence, electricity and water are produced through means of series of chemical reactions and physical processes.

Theoretically, a fuel cell can convert more than 80% of the energy into usable electric power and heat [5]. Therefore, fuel cells have the potential of providing advantages in high efficiency, high power density, no fossil fuel dependence, safe and enviromentally friendly operation.

1.2. Fuel Cells

The first fuel cell principle was discovered by William Robert Grove and reported in 1839 [6]. The invention was based on the idea that the electrolysis of water requires energy to produce the hydrogen and oxygen gas. Grove introduced the first hydrogen-oxygen gas fuel cell using sulfuric acid electrolyte and a platinum electrode. The experimental set up of Grove included the cells containing gaseous hydrogen and oxygen to produce the electron flow to upper cell. Hence, the energy produced from bottom cell was used for the electrolysis of water producing gaseous hydrogen and oxygen (Figure 1.4).

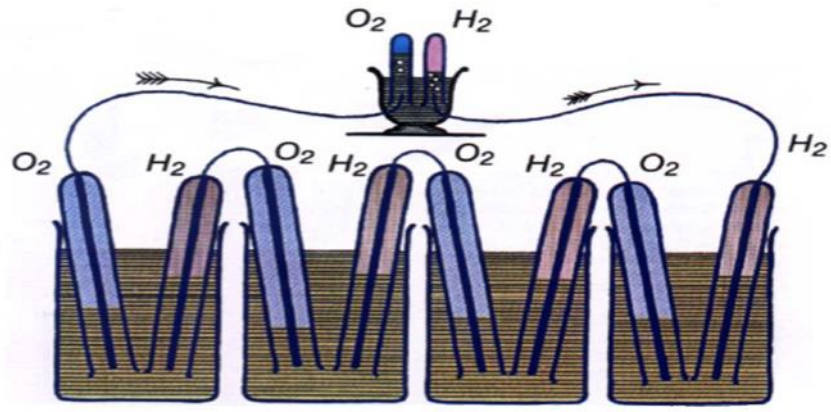

Figure 1.4. The first fuel cell introduced by William R. Grove.

After this discovery followed nearly a century of research attempts to improve Grove's cell into a practical device. It was Francis Thomas Bacon, who started researching alkali electrolyte fuel cells (with potassium hydroxide) in the late 1930s, that demonstrated in the late 1950s the first large scale fuel cell stack. Bacon's fuel cells attracted the attention of Pratt & Whitney who licensed his work to power the Apollo spacecraft.

Low temperature proton exchange membrane fuel cell (PEMFC) technology was invented later at General Electric in 1955, through the work of Thomas Grubb and Leonard Niedrach. The PEMFC was the first type of fuel cell to have an application. It was used as a power source for NASA's Gemini space flights in the 1960s [7]. The formation of the

California fuel cell partnership for the development and commercialisation of zero-emission vehicles stimulated the research on PEMFCs.

At the beginning the cell was quite expensive to produce as the catalyst electrodes used Pt and the Pt loading was as high as 30 mg Pt cm^{-2} [8]. In the early 1990s the Pt loading was dramatically reduced to approximately 0.5 mg Pt cm^{-2} by supporting the Pt particles on a graphitic carbon support, which greatly increased the catalytic surface area and then the performance [9]. The catalyst layer was directly bonded to membrane. This breakthrough combined with the raise of the energy cost led to active research and development on PEMFCs which continues today.

Nowadays, fuel cells have much wider applications than any other currently available power sources from toys to large power plants. According to the U.S. Department of Energy, "Fuel cells are primary candidates for light-duty vehicles, for buildings, and potentially for much smaller applications such as replacements for rechargeable batteries." Hence, it would be reasonable to argue that there will be a bright future for the fuel cells.

1.2.1. Types of Fuel Cells

Fuel cells are categorised according to their type of electrolyte. The six main types of fuel cells are given below:

- Alkaline Fuel Cells (AFC),
- Phosphoric Acid Fuel Cells (PAFC),
- Molten Carbonate Fuel Cells (MCFC),
- Solide Oxide Fuel Cells (SOFC),
- Direct Methanol Fuel Cells (DMFC),
- Proton Exchange Membrane Fuel Cells (PEMFC).

Fuel Cell types are summarized in Table 1.1 [10].

Table 1.1. Types of fuel cells.

Fuel Cell Type	AFC	PAFC	MCFC	SOFC	DMFC	PEMFC
Electrolyte	KOH	H_3PO_4	Li_2CO_3 + K_2CO_3	ZrO_2 + Y_2O_3 (YSZ)	Polymer	Polymer
Charge Carrier	OH^-	H^+	CO_3^{2-}	O^{2-}	H^+	H^+
Fuel	Pure H_2	CO free H_2	H_2 and hydrocarbons	H_2 and hydrocarbons	CH_3OH	Pure H_2
Operating Temperature(°C)	65-220	150-220	600-800	500-1000	50-120	80-200
Power Range (W)	10-100k	100-400k	300k-3M	1k-2M	20-5k	1-100k
Efficiency (%)	35-40	30-40	60-70	40-70	40	40-60

1.3. Proton Exchange Membrane Fuel Cell (PEMFC)

The proton exchange membrane fuel cell (PEMFC), also called polymer electrolyte membrane fuel cell, typically use pure hydrogen as a fuel to generate electricity. In the PEMFC, the hydrogen fuel combines with the oxygen from the atmosphere to produce water, electricity and heat. The most important part of a PEMFC is the membrane electrode assembly (MEA). The membrane is solid polymer electrolyte, which is bonded to catalyzed porous electrodes (anode and cathode) placed on each side. Both anode and cathode are usually composed of a Pt-containing catalyst on conductive carbon.

The PEMFC was developed in the early 1990s. However, the PEMFC was not approved in that decade due to its low efficiency and power density. After the efficiency of PEMFC was improved to more than 50%, it has been started to be used as a primary energy sources for different systems [11]. The PEMFC has been generally regarded as an efficient and convenient power source for portable power applications, such as mobile phones and laptop computers.

Solid polymer membrane is used as an electrolyte in PEMFC. Protons can penetrate from the polymer which does not conduct electrons. The chemical reactions and the flow of electrical current are shown in Figure 1.5 [12].

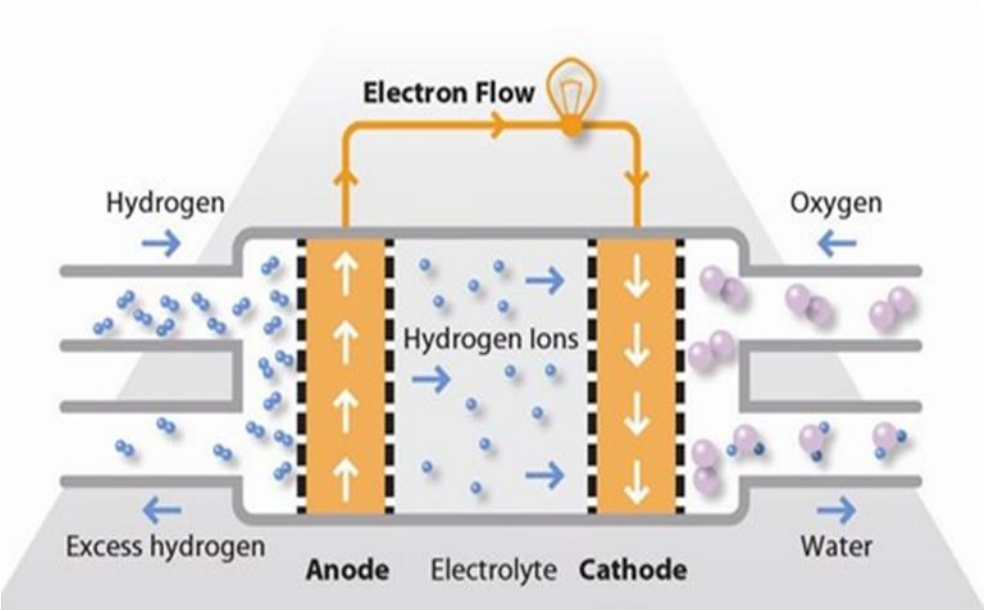

Figure 1.5. The diagram of a proton exchange membrane fuel cell.

The operation of fuel cell can be explained like this: on the anode side, the hydrogen molecule is split into protons and electrons. The protons flow across the electrolyte to the cathode side while the electrons move through an external circuit. On the other side, oxygen is pumped into the fuel cell on the cathode side. At the top of the picture, the anode and cathode sides are connected by an electrical circuit. These electrons move to the cathode side through the electrical circuit. The protons and electrons will be combined with oxygen to form water on the side of cathode. The excess water goes out when the action runs regularly.

The reaction equation of PEMFC is [13]:

Anode : $2H_2 \longrightarrow 4H^+ + 4e^-$

Cathode : $O_2 + 4H^+ + 4e^- \longrightarrow 2H_2O$

Overall : $2H_2 + O_2 \longrightarrow 2H_2$

Compared to other types of fuel cells, PEMFCs generate more power for a fixed weight of fuel cell. The high-power density characteristic makes them compact and light-weight. In addition, the operating temperature is nearly 100 °C, which allows a rapid start-up. Compared to many other fuel cells, the PEMFCs lead to a longer operating life. They are easy to design and adaptable in size. In addition, the PEMFCs have solid non-corrosive polymer electrolyte. Therefore PEMFCs are adopted by major auto makers [14].

One of the disadvantages of PEMFC is its low operating temperature. Temperatures near 100 °C are not high enough to perform useful cogeneration. Another limitation for the wide use of PEMFCs is high manufacturing cost due to polymer membrane. PEMFCs are sensitive to carbon monoxide and pure hydrogen is needed [15].

The applications of PEMFCs can be classified into two classes. One is a settled power supply, the other one is a portable power supply.

PEMFC is applied in large-scale power plants. However, due to the restrictions of the manufacturing cost and fuel, PEMFC cannot be used in central power stations [16].

PEMFC used as a portable power supply is suitable for military, computer, geology, microwave station, meteorological observatory, communication, financial market, hospital and other fields. It is widely used in transportation such as motorcycle, car, train, ship, owing to satisfying the environmental requirements [17].

1.3.1. Polymer Membrane as Electrolyte

In PEMFCs, the membrane is the core component because it provides a conductive path for the protons but separates the two electrodes electronically. The polymer membrane is acting not only as an electronic insulator between anode and cathode but also gas barrier to prevent mixing of hydrogen and oxygen. To achieve high efficiency the membrane must have following properties [18]:

- high proton conductivity to support high currents with minimal resistive losses and zero electronic conductivity,

- adequate mechanical strength and stability,
- chemical and electrochemical stability under operating conditions,
- moisture control in stack,
- extremely low fuel or oxygen by-pass to maximize coulombic efficiency,
- production costs compatible with intended application.

Figure 1.6 gives classification of the membrane materials which are used in PEMFCs [19].

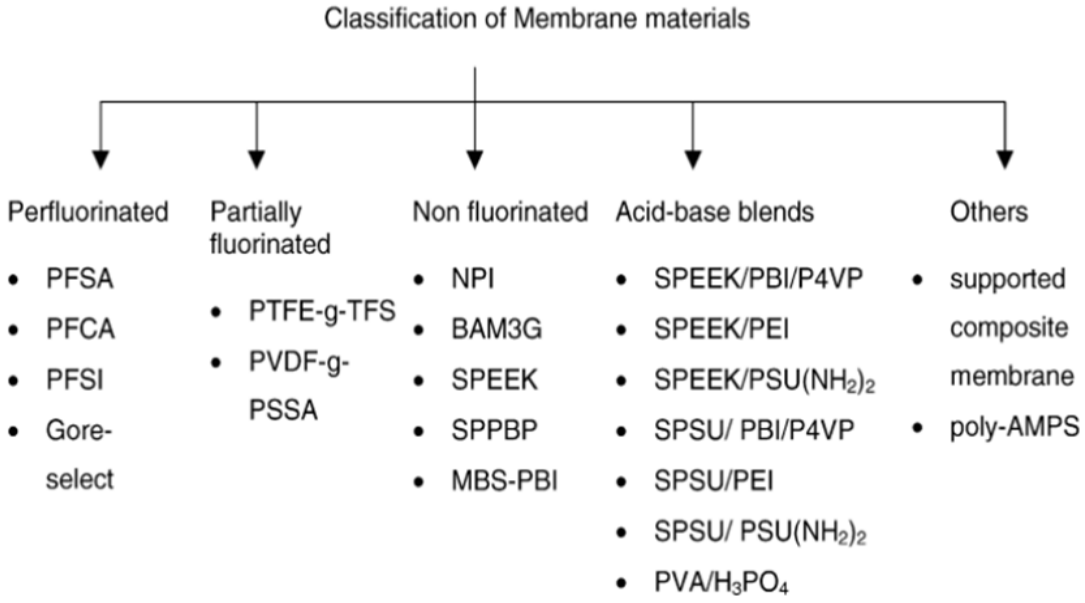

Figure 1.6. Classification of membrane materials.

In PEMFCs, Perfluorosulfonic acid (PFSA) membranes are commonly used. The PFSA membrane is produced more extensively by DuPont. The commercial name is Nafion. The Dupont product is considered to be superior due to its high proton conductivity, good chemical stability and mechanical strength. The structure is shown in Figure 1.7 [20].

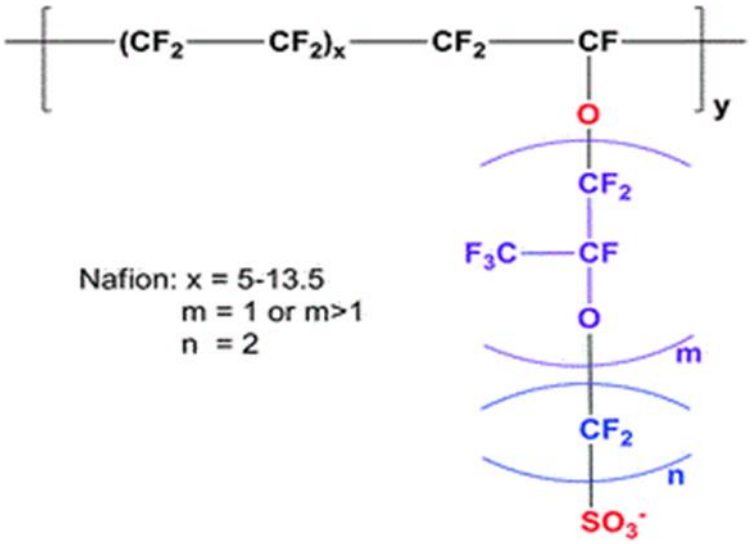

Figure 1.7. Chemical structure of Nafion.

Proton conductivity in Nafion changes due to variation in operating parameters such as temperature (~100^{o}C), membrane thickness and water content. However, there are several disadvantages of Nafion which are as the following [21]:

- the high cost of membrane amounting to US$ 700 per square meter,
- lack of safety during its manufacture and use,
- requirement of supporting equipment,
- temperature related limitations [22].

The other membrane materials are listed above (Figure 1.6) and researchs are proceeded without slowing down to improve and develop membrane materials with better properties. Beside the shortcomings of Nafion, it is still the polymer choice for most PEMFC applications. It is likely that Nafion will be replaced by an alternative membrane in the future.

1.3.2. Electrodes

The electrodes are another critical components in PEMFCs. As described above, the hydrogen fuel is splitted into protons and electrons at the anode electrode, and the oxygen

reacts with protons and electrons to produce water at the cathode electrode. The performance and durability of the fuel cell is dependent on the electrodes as well as the membrane. Platinum is widely used as catalyst material both at the anode and cathode sides [23].

The hydrogen oxidation kinetics on Pt catalyst is very fast, therefore, lowering Pt loading for anode is straightforward. The kinetics is only controlled by mass transfer. The hydrogen oxidation occurs in several sub-steps including adsorption and dissociation of the molecule into two H^+ ions. The reaction is indicated below [24];

$$2Pt + H_2 \longrightarrow Pt\text{-}H_{ads} + Pt\text{-}H_{ads}$$

$$Pt\text{-}H_{ads} \longrightarrow H^+ + e^- + Pt$$

However, the reduction of the Pt-loading for the cathode is limited due to the poor activity of Pt towards O_2 reduction [25].

In the fuel (H_2 gas), there are some contaminants such as carbon monoxide, sulfur and ammonia which reduce catalytic activity of Pt catalyst. The carbon monoxide adsorption on active sites of platinum decreases the catalytic activity with time and catalytic activity eventually disappears. Carbon monoxide poisoning can be avoided by fuel reforming or catalyst alloying techniques. Fuel reforming includes the addition of hydrogen peroxide to the fuel. Catalyst alloying technique includes platinum alloys of Re, Ru, Os, Rh, Mo, Pb, Bi and Sn have been well studied to oxidize the carbon monoxide to carbon dioxide [26].

However, the cost of the electrodes is about 40% of the total cost in manufacturing fuel cell [27]. The high cost of the electrodes is mostly due to the expensive platinum catalysts. Pt based catalysts could be black Pt powders or carbon supported Pt particles. Pt is the best catalyst for fuel cell from past to present because Pt is the most active, efficient and successful catalysts [28].

There are two general approaches to reduce the cost of the catalysts: reduction of the Pt loading and development of non-noble catalysts [29,30]. In recent years, there has been significant activity in developing new and lower cost non-noble catalysts, such as metal-

based catalysts and nanostructure catalysts. The conventional catalyst layers generally featured expensive platinum loadings of 4 mg/cm^2. A generous amount of research has been directed at reducing Pt loading below 0.4 mg/cm^2 [31,32]. Recently, platinum loadings as low as 0.014 mg/cm^2 have been reported using novel methods [33,34].

The studies are conducted to reduce the amount of platinum used in fuel cells. Not only is it important to lower Pt loading in order to reduce fuel cell cost but also it is essential to maintain the activity of Pt catalysts during the lifetime of fuel cells. As a consequence of this focused effort, the cost of the catalyst is no longer the major barrier to the PEM fuel cells commercialization. One way of reducing the quantity of the metal is to reduce the size of Pt nanoparticles [35]. Nanoparticles can display several advantages over electrode producing; high effective surface area, enhancement of mass transport and low cost. The increase of relative surface area is a critical factor for efficient catalysis and electrodes [36].

1.4. Nanoparticles

Nanoparticles range in size from about 100 nm down to about 1 nm. They show novel properties different from their bulk materials. Studies on nanoparticles to develop new materials and their applications are generally called nanotechnology.

In recent years, nanoparticles have been the center of researchers' attention, because they have a very large surface area compared to their volume. Hence, they are often able to make the reactions possible in milder conditions. This makes them useful as catalysts to speed up reactions. Nanoscience may lead to the development of [37]:

- new coatings,
- new computers,
- stronger and lighter building materials,
- sensors that detect individual substances in tiny amounts,
- new catalysts.

Researchers have been employing nanoparticles to develop the low cost electrodes as fuel cells. These electrodes may be able to replace the expensive platinum which is needed as fuel cell catalysts. For instance, catalysts using platinum-cobalt, platinum-nickel, and platinum-copper nanoparticles have been developing for fuel cells which have more catalytic activity than pure platinum. In order to achieve this performance, researchers anneal nanoparticles to form them into a crystalline lattice, reducing the spacing between platinum atoms on the surface and increasing their reactivity [38].

The transition from microparticles to nanoparticles is seen to cause excellent changes in the physical and chemical properties of a material. The most important characteristics on a nanoscale are as follows; first, the small size of particles bring an increased surface area and as a result domain where quantum effects predominte is entered. Second, the increasing surface area to volume ratio leads to increase in dominance of the surface atoms of the nanoparticle over those in its interior.

Approaches for nanomaterial synthesis can be divided into two categories; “top-down” and “bottom-up”. The “top-down” approach is used to cut, mill and shape materials into the desired shape and order. Most common techniques are lithographic techniques (e.g. UV, electron or ion beam, scanning probe and optical near field), laser beam prossessing and mechanical techniques (e.g. machining, grinding and polishing). On the other hand, “bottom-up” approaches are chemical synthesis, chemical vapor deposition, laser induced assembly, self assembly, colloidal aggregation, film deposition and growth.

There are a wide range of techniques for synthesizing different kinds of nanoparticles. These techniques are classified into three categories:

- Condensation from vapor,
- Synthesis by chemical reaction,
- Solid state processes such as milling.

By using the above mentioned techniques, pure nanoparticles, hybrid and coated nanoparticles which are hydrophilic or hydrophobic materials depending on the convenience of the applications can be synthesized.

Primarily, researchers studied single nanoparticles due to their superior properties over the bulk materials. In the late 1980, researchers found heteregeneous, composite or sandwich collaidal semiconductor particles which have better efficiency than their

corresponding single particles. In the early 1990s, researchers improved such semiconductur materials and developed concentric multilayer semiconductor materials. Subsequently, the terminology core-shell was embraced. Moreover, there has been a great research activitiy due to the tremendous demands of modern technology.

Nanoparticles can be classified based on single or multiple materials into simple and core-shell or composite nanoparticles. Generally, simple nanoparticles are produced a single material, while core-shell and composite nanoparticles comprised of two or more materials. The core-shell nanoparticles can be defined as composing a core which is an inner material and a shell which is an outer layer material. There are a wide range of different combinations including inorganic and inorganic, inorganic and organic, organic and inorganic, organic and organic materials. The choice of shell material depends on the end application and usage. However, with the advanced techniques not only symmetrical (spherical) shape nanoparticles but also a wide variety of other shapes such as cube, prism, hexagon, octahedron, disk, rod etc. are synthesized. The properties of nanoparticles are not only size dependent but also linked with the shape. Different shape core-shell nanoparticles have also given rise to extensive research interest owing to a wide variety of novel properties. Currently simple nonspherical and different shape core-shell nanoparticles are broadly reported in articles [39-43].

1.4.1. Core-Shell Nanoparticles

Core-shell nanoparticles are made of two or more different metal nanoparticles in which one metal completely surrounds another metal creating a core and shell structure (Figure 1.8). The inside material, known as the core, is completely covered with the shell metal, so it is not exposed for chemical reactions.

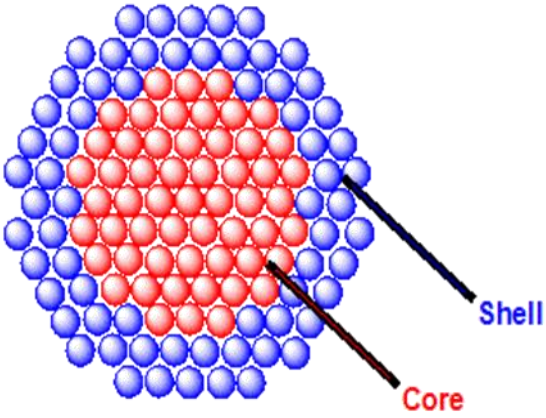

Figure 1.8. Core-shell nanoparticle structure.

This core-shell nanoparticles are made of an inexpensive metal core and a noble metal shell have received particular interest because of the functional and economic advantages that they can provide. Through modified properties, core-shell nanoparticles have been developed highly functional materials. Sometimes physical and chemical properties arising from either core or shell materials can be quite different from their original metallic character. The properties can be modified by changing the constituting materials or the core to shell ratio. The purpose of the coating on the core particle are many fold, such as surface modification, the ability to increase the functionality, stability, and dispersbility, controlled release of the core, reduction in consumption of precious materials, etc.

The core-shell nanocomposites and nanostructure may be in different sizes and different shapes of core and shell thickness with different surface morphology. Different classes of core-shell nanoparticles are shown in Figure 1.9. Concentric spherical core-shell nanoparticles are the most common (Figure 1.9a) where a simple spherical core particle covered by a shell of different material. Another shaped core-shell nanoparticles are generally formed when a core is nonspherical as shown in Figure 1.9b. Multiple core-shell nanoparticles are formed when a single shell material coated onto many small core particles together as shown in Figure 1.9c. Alternative coating of dielectric core and metal shell material onto each other are shown in Figure 1.9d. It is also possible to synthesize a moveable core particle within a hollow shell particle after a bilayer coating of the core material and removing the first layer by using the suitable technique (Figure 1.9e) [44].

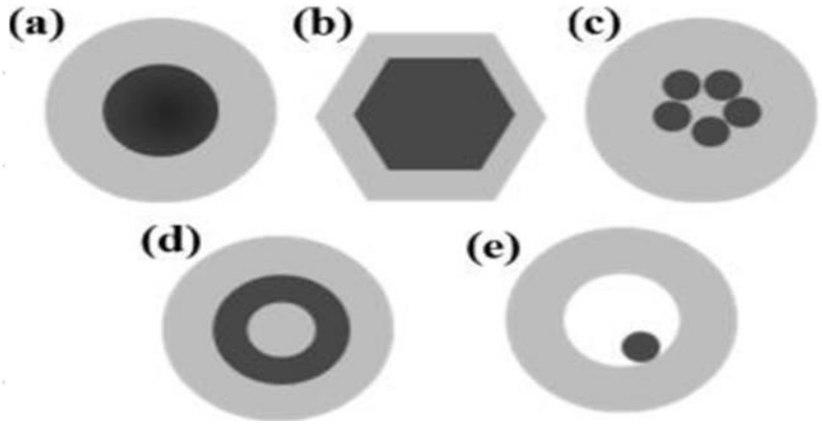

Figure 1.9. Different core-shell nanoparticles.

Core-shell nanoparticles are gradually attracting more and more attention day by day. In recent years, core-shell nanoparticles used for fuel cell electrode synthesis due to functional and economical advantages. Depending on the size and shape, their properties change from one material to another. The individual reports from different researchers demonstrate that core-shell nanoparticles are widely used in different purposes such as microvessels, catalyst supports, adsorbents, lightweight structural materials, thermal and electric insulators, biomedical and pharmaceutical applications, enhancing photoluminescence, creating photonic crystals, etc.

In addition to the improved material properties, core-shell materials are also important from an economic point of view. A precious material can be coated over an inexpensive material to reduce the consumption of the precious material compared with making the same sized pure material. Core-shell nanoparticles with very thin noble metal shells have a great significance in chemical catalysis. Noble metals (e.g.Pt, Pd) are excellent and versatile catalysts in various reactions. However, they occur in nature very low levels of abundance. Arranging noble metals as thin (ideally monolayer) shells on proper nonnoble metal cores not only greatly reduces their use, but also could significantly enhance their catalytic properties via the so-called strain and ligand effects of the core substrate on the supported noble metal overlayer [45].

1.4.2. Fuel Cell Applications of Core-Shell Nanoparticles

There are a variety of core-shell nanoparticle reports which used as catalysts in PEMFCs. Ni-Pt, Cu-Pt, Co-Pt, Ru-Pt, Pd-Pt are mostly used ones. Ru@Pt nanoparticles show an increased availabilty of CO-free Pt surface sites and remarkable improvement of catalytic activity. Pd@Pt core-shell structures have near surface alloy effects in which subsurface metal and alloy layers affect the binding enthalpies. The changes in binding enthalpies can cause an enhancement in selectivity in catalytic process. In addition both Ni@Pt, Co@Pt and Cu@Pt core-shell nanoparticles have reduced content of Pt and they exhibit enhanced catalytic activity compared to pure Pt catalyst [46].

However, combination of Ag and Au is extensively used in optical studies. Metal core dielectric shell nanoparticles another example of core-shell applications such as metal core SiO_2 shell and metal core TiO_2 shell nanoparticles are used in solar cells, high density information storage systems and electrochromic devices [47].

Moreover, there are multi-shell structure systems. These systems involve a non-noble metal core (Co, Ni), a noble metal protective shell (Au, Pd, Pt) and a Pt overlayer. The system provides greatly enhanced Pt-mass activity. Figure 1.10 shows several types of core-shell nanoparticles [48].

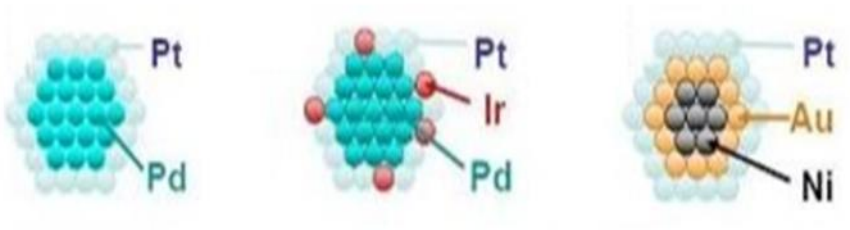

Figure 1.10. Different types of core-shell nanoparticles.

2. AIM OF THE STUDY

The work presented in this thesis will focus on the development of core-shell nanoparticles as the catalyst for PEM fuel cells. For catalyst, there are two different ways to synthesized core-shell nanoparticles. First one is to synthesize a thin layer of platinum shell on a transition metal core in which nickel, copper and cobalt are used. Other one is to synthesize both core and shell together then remove from the noble metal which is nickel on the surface with acid treatment.

The aim of this project is not only greatly reduce the amount of Pt loading but also could enhance the catalytic properties via strain and ligand effects of the transition metal core on the Pt shell. Core-shell nanoparticles are synthesized by the reduction of metal salt. In this project sodium borohydride is used.

There are two different kinds of core shell model synthesized. First one is type 1 and other one is type 2, which is shown in Figure 2.1.

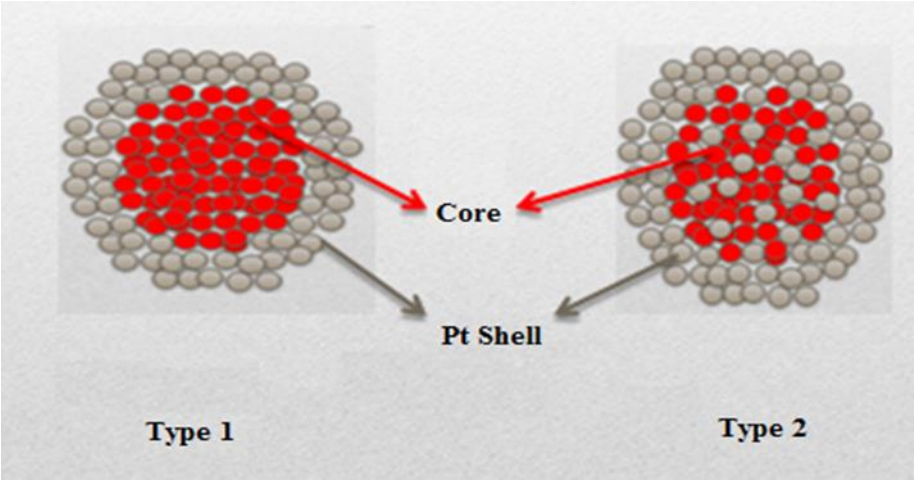

Figure 2.1. Different types of core-shell synthesis.

For type 1, there is a platinum shell and transition metal core and for type 2 there is a platinum shell and both transition metal and platinum core. Sub 10 nm core-shell nanoparticles are aimed to synthesize. Both electrochemical (CV, RDE and activity measurements) and analytical (TEM, XPS, XRD) techniques will be used in order to elucidate the catalyst structure and test their activity and stability.

3. EXPERIMENTAL

3.1. Reagents

The chemicals and materials, used for synthesis, are listed in the Table 3.1.

Table 3.1. Chemicals and materials used in this work.

Name	Suppliers	Purity or Noted
H_2PtCl_6	Sigma-Aldrich	99.9%
$NiCl_2.6H_2O$	Sigma-Aldrich	98%
$Ni(Ac)_2.4\ H_2O$	Sigma-Aldrich	98%
NaOH	Merck	99%
Oleic Acid	Sigma-Aldrich	>99%
1,2 Propanediol	Sigma-Aldrich	ACS
$NaBH_4$	Sigma-Aldrich	99%
$Cu(Ac)_2$	Sigma-Aldrich	98%
PVP_{K58}	Alfa-Aesar	MW 58000
Ethylene Glycol	Alfa-Aesar	99%
$CoCl_2.6H_2O$	Ridel	99%
Ethanol	Merk	ACS
Propan-2-ol	Merck	99.5%
Carbon Support	Vulcan XC72	
Nafion	DuPont	

3.2. Synthesis Of Core-Shell Nanoparticles

3.2.1. Synthesis of Nickel $_{core}$ – Pt $_{shell}$ Nanoparticles (Ni@Pt)

To prepare nanosized nickel nanoparticles, 0.9 g NaOH and 1 mL oleic acid and 0.08 g $Ni(Ac)_2$ were mixed in 50 mL of 1,2 propanediol solution. The solution was heated and stirred to 118^oC for 20 minutes until the bright green solution was obtained. Then, the solution was heated and stirred to 138^oC for 20 minutes, the bright green solution turned dark green nearly brown.

At which point 0.23 g $NaBH_4$ was solved in 10 mL of 1,2 propanediol solution and slowly added the reaction flask. However, there was another way to prepare reduction solution which is same amount of $NaBH_4$ was solved in 6 mL isopropyl alcohol and 4 mL deionized water and then slowly added the reaction flask. The solution turned black upon the addition of $NaBH_4$ solution. The black solution indicates the formation of Ni nanoparticles. The reaction process was carried under N_2 atmosphere to prevent oxidation of the Ni nanoparticles.

After formation of Nickel nanoparticles, the solution was aged for about 20 minutes under stirring and N_2 atmosphere at 138 ^oC. Freshly prepared 3 mL 1,2 propanediol and 0.008 g H_2PtCl_6 was added dropwise. The reaction solution was continously stirred for 30 minutes and at the end of the time cooled to room temperature under N_2 atmosphere (Figure 3.1) [49].

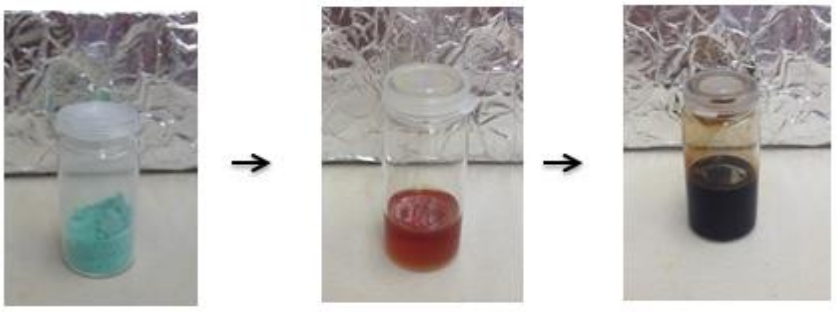

Figure 3.1. Ni@Pt/C core-shell synthesis.

3.2.2. Synthesis of Cobalt $_{core}$ - Pt $_{shell}$ Nanoparticles (Co@Pt)

0.105 g $CoCl_2.6H_2O$ in 10 mL ethanol solution was mixed with 0.07 g Poly-vinyl pyrrolidone (PVP) in 10 mL ethanol solution. Then, freshly prepared 0.2g $NaBH_4$ and 0.1 g NaOH in 10 mL ethanol was added dropwise with stirring. The solution was stirred for 30 minutes at room temperature. Co nanoparticles are synthesized using reduction method. $NaBH_4$ and NaOH, a strong reduction agent, was used to quickly reduce part of the Co^{2+} to form Co nanoparticles. Poly-vinylpyrrolidone was used as stabilizer to control particle size.

Pt was then deposite onto Co using the following method. 0.007 g H_2PtCl_6, 0.002 g $NaBH_4$ and 0.001 g NaOH are mixed with 5 mL ethanol and added the solution. Then, the solution was heated at 60^oC under vigorous strring during 3 hours. At the end of the experiment Co core Pt shell solution was cooled to room temperature.

The $CoCl_2.6H_2O$ is purple and with the addition of PVP, the solution turned into dark blue. After the mixing with $NaBH_4$, the solution turned into black. The black solution indicates Co nanoparticles. If pH conditions do not adjusted properly, instead of forming metal nanoparticles, Co^{2+} inclines to compose of cobalt boride. NaOH has a great importance to stabilize the pH [50].

3.2.3. Synthesis of Copper $_{core}$ - Pt $_{shell}$ Nanoparticles (Cu@Pt)

For the preparation of Copper nanoparticles following method was used. 0.050 g $Cu(ac)_2$ and 0.025 g Poly-vinylprrolidone (PVP) was dissolved in 40 mL ethylene glycol (EG) at 80^oC with stirring. At this point solution was bright green.

In second step, 0.2 g $NaBH_4$ and 0.1 g NaOH in 10 mL ethylene glycol was added the solution. With the addition of reduction agent $NaBH_4$ solution color changed from bright green to black. After the solution was slowly heated to 160 ^oC and aged 3 hours under vigorously strring. Stirring was quite important to prevent agglomeration.

For Pt shell deposition, 0.006 g H_2PtCl_6, 0.002 g $NaBH_4$ and 0.001 g NaOH were mixed with 5 mL ethylene glycol and added the solution. The solution was heated to 130^oC and aged 4 hours [51].

3.2.4. Acid Treated Ni $_{core}$ – Pt $_{shell}$ with Carbon Support (Ni@Pt/C) Core-Shell Synthesis

Low temperature reduction method was used to synthesize nickel and platin nanoparticles. Initially 500 mL $H_2PtCl_6.H_2O$ solution was prepared with 2.5 g $H_2PtCl_6.H_2O$ and deionized water and 500 mL $NiCl_2.6H_2O$ solution was prepared with 25 g $NiCl_2.6H_2O$ and deionized water. Then 1:1 ratio in mass $NiCl_2.6H_2O$ and $H_2PtCl_6.H_2O$ solutions were mixed in a beaker for synthesized 50 mg catalyst material. They were stirred for 30 minutes. After 50 mg C black which is Vulcan XC-72 was suspended in 10 mL ethanol-water solution. 75 mg $NaBH_4$ is solved in 10 mL deionized water and mixed with the C black solution. The mixed solution was rapidly stirred for 5 minutes. After stirring the solution, it is quickly added the nickel and platin solution. Then, it is stirred for 30 minutes. The product was collected by centrifuge (6000 rpm, 20 min). The obtained NPs were further washed by deionized water until there is no chloride in the solution. To understand removal of the chloride $AgNO_3$ testing applied. After these processes the catalyst product were dried at 70^oC for 24 hours.

The obtained catalyst was denoted as PtNi/C. At the end of the process Ni-Pt nanoparticles were synthesized but they were not in core-shell structure. To obtained core-shell structure, acid treatment was neccessary. For the acid treatment, all the prepared PtNi/C catalyst were mixed with 50 mL 0.5 M H_2SO_4. After 2 nights exposured to the acidic environment, the product was collected by centrifuge and washed by deionized water. Such nanoparticles were named acid treated PtNi/C core-shell nanoparticles which in core Pt-Ni and at shell Pt nanoparticles were founded (Figure 3.2) [52].

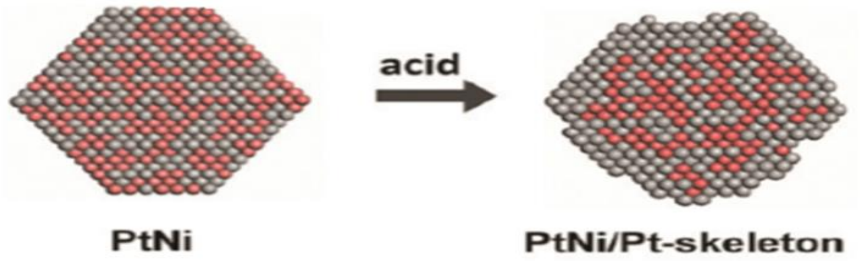

Figure 3.2. Acid treated Ni@Pt/C catalyst with core-shell structure.

3.3. Techniques For Electrochemical Characterization

3.3.1. Cyclic Voltammetry (CV)

Cyclic voltammetry is a very useful tool for surface characterisation. Cyclic voltammetry is generally called CV. To perform CV measurements, a three-electrode cell configuration shown schematically in Figure 3.3 which is usually used. It consists of three electrodes immersed in electrolyte which are working electrode (WE), the counter electrode (CE) and the reference electrode (RE).

3.3.1.1. Working Electrode (WE). The potential applied to the working electrode. It is swept back and forth between two chosen limits. The working electrode is the electrode where oxidation and reduction processes are happened. The obtained voltammogram is a plot of current, i, versus potential, E, which is time-dependent. The potential of the WE is measured against the RE and the current is passed between the WE and CE. The counter electrode makes a connection to the electrolyte until a current can flow between the working and the counter electrodes when a potential is applied to the working electrode.

3.3.1.2. Reference Electrode (RE). The effects of adsorbing anions on the rate of oxygen reduction reaction (ORR) places restrictions on the choice of reference electrode, which being in direct contact with the electrolyte should not contain any adsorbing species. In particular, electrodes containing Cl^- and SO_4^{2-} should be avoided, which rules out the common saturated calomel (SCE), silver/silver chloride (Ag/AgCl) and mercury sulphate (MSE) electrodes. Although the reference electrode can be separated from the bulk electrolyte by a salt bridge, the rate of diffusion of ions through the bridge is still finite, and therefore an alternative reference electrode is desirable, especially for long experiments. The Reversible Hydrogen Electrode (RHE) is a convenient non-contaminating reference electrode for studies on ORR catalysts. It consists of a Pt wire, gauze or foil in direct contact with both an acidic electrolyte and gaseous H_2, establishing a triple-phase boundary at which the equilibrium in (3.1) is established, providing a reference potential against which the working electrode Polarization can be measured. It

happens that, by convention, the equilibrium in (3.1) is designated a standard electrode potential of 0.0 V.

$$H_2(aq) \Leftrightarrow 2H^+_{(aq)} + 2e^-_{(aq)} \qquad E^0 = 0.0V \qquad (3.1)$$

The RHE contains no adsorbing anions, so there is no contamination risk to the experiment.

3.3.1.3. Counter Electrode (CE). The function of the counter electrode is simply to generate an equal and opposite current to that flowing to the working electrode, so that the reference electrode can remain at equilibrium. Pt is often chosen as a counter electrode material, as it is inert and will not decompose electrolytically to contaminate the electrolyte. The counter electrode potential is controlled by the potentiostat and can vary by up to ±50 V vs the working electrode (the maximum potential difference is known as the compliance voltage). Although for typical experiments where working electrode currents are of the order of < 1 mA, such extreme potential differences are rarely required. Nevertheless, for ORR experiments in HClO4 it is important to minimise the counter electrode Polarization to avoid contamination of the electrolyte via unwanted reactions such as:

$$ClO_4^-{}_{(aq)} + 8H^+ + 7e^- \Leftrightarrow \tfrac{1}{2}Cl_{2(g)} + 4H_2O_{(aq)} \qquad E^0 = 1.42\ V \qquad (3.2)$$

Indeed, it is desirable to limit the magnitude of any Faradaic currents on the counter electrode, and ensure that any reactions occurring at its surface are not mass-transport limited, by ensuring that its active surface area is an order of magnitude larger than that of the working electrode.

3.3.1.4. Electrolyte Section. For absolute determination of catalytic activity towards ORR, it is important that the electrolyte is non-adsorbing; there should be no component or

impurity in the electrolyte that can undergo specific adsorption to Pt surfaces, and in doing so block active sites and reduce the observed kinetic current density. Many common electrolytes are therefore unsuitable for measurement of ORR kinetics. Notably, the bisulfate (HSO_4^-) anion can block Pt surface sites by undergoing specific adsorption, particularly to Pt (111) type fcc surfaces. The same is true of halide anions, including chloride (Cl^-). Perchloric acid ($HClO_4$) is non-adsorbing and is therefore commonly employed in the characterisation of PEMFC electrocatalysts.

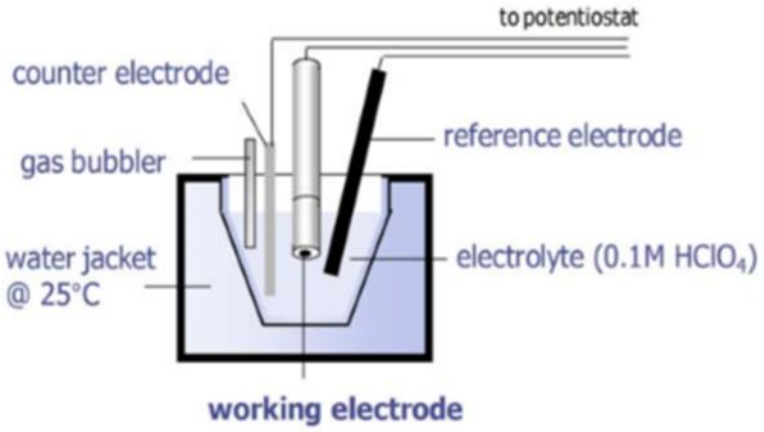

Figure 3.3. Electrical circuit for a three-electrode cell.

3.3.1.5. Characterization of Metal Surfaces. Cyclic voltammetry is very useful for catalyst surface characterisation as a surface sensitive technique. When the potential is reached to the upper limit, oxidation process occur at the electrode. When the potantial is reached to the lower limit, reduction process occur at the electrode. In acidic aqueous electrolyte, noble metals absorb hydrogen and oxygen by charge transfer. However, the shape and the potential of the corresponding features are characteristic of the metal.

In Figure 3.4, between 0 and 0.4 V, hydrogen is adsorbed on the cathodic sweep and oxidized on the anodic sweep. It is giving rise to two pairs of peaks. These peaks are assigned to weakly and strongly bound hydrogen. The desorption-adsorption of hydrogen occurs through the reaction:

$$M\text{-}H \quad \Leftrightarrow \quad M + H^+ + e^+$$

In the double-layer region 0.4 and 0.8 V, no electrochemical reaction happens and the current recorded is due to the accumulation of charges from the electrolyte at the polarized interface. Above 0.8 V, oxygen starts to be chemisorbed and oxides are formed. As the potential increases above 0.8 V, the oxygen adsorption becomes progressively irreversible due to rearrangement of the oxygen species layer into two dimensional lattice of O species and metal atoms. At the beginning of the oxide formation, the Pt surface interacts with the O-containing species present in the electrolyte (H_2O, OH^-) and as the process proceeds a three-dimensional oxide lattice develops.

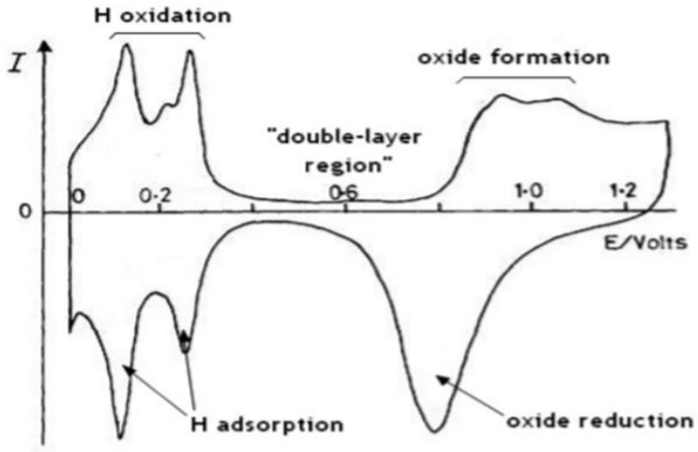

Figure 3.4. Cyclic voltammogram of a Pt electrode in 0.5 M H_2SO_4.

The active surface area of a metal can be calculated from cyclic voltammetry in acidic media. The active surface area (m^2/gPt) is:

The Active Surface Area = Average Area/0.21.Charge.Scanning Rate

3.3.1.6. Experimental. I completed all of the cyclic voltammogram measurements at the Gebze Yüksek Teknoloji Enstitüsü with using a Pine Instrument Company, bipotantiostat model AFCBP1.

For preparation of the electrodes, 0.196 cm^2 disk-electrodes were prepared by brush-coating an aqueous based catalyst ink. To prepare catalyst ink, 0.35 mg synthesized catalyst and 0.23 mL deionized water, 0.69 mL isopropyl alcohol and 0.013 mL 7% Nafion solution were used.

For electrochemical measurements, the electrochemical study was carried out in standart three electrode cell using a Pine Instrument Company, bipotantiostat model AFCBP1 (Figure 3.5). The reference electrode used was Ag/AgCl. This electrode was choosen due to having better resistance than standart hydrogen electrode (SHE). At the end of the experiment required calculations were performed. A Pt coil served as the counter electrode. A cyclic voltammogram was run in 0.5 M H_2SO_4 between -280 - 1200 mV at 100 mV s^{-1} (N_2 atmosphere).

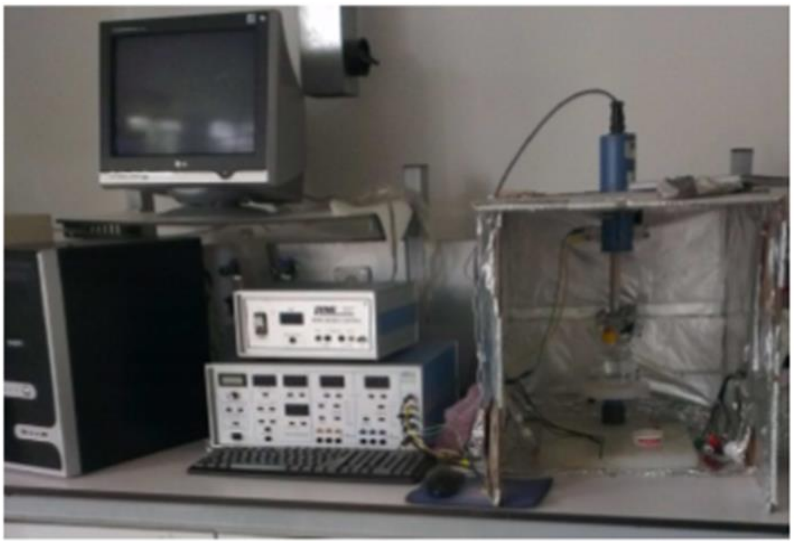

Figure 3.5. Cyclic voltammetry (CV).

3.3.2. Rotating Disk Electrode (RDE)

The Rotating Disk Electrode (RDE) is the classical hydrodynamic electroanalytical technique which used to limit the diffusion layer thickness. The RDE consists of a disk (such as Pt or glassy carbon) set into an insulating (PTFE) surround. The electrode is rotated about its vertical axis, typically between 400 and 10000 rpm. Similar to cyclic

voltammetry, in rotating disk voltammetry, the potential of the working electrode is swept back and forth between two potential limits. The difference between cyclic voltammetry and rotating disk electrode is that the working electrode is rotated at a very high speed. The motion induces a well-defined flow pattern of the electrolyte, where it is pumped up from the bulk towards the electrode surface and then flung out centrifugally. The layer of liquid adjacent to the electrodes is motionless with respect to the electrode and rotates at the same velocity. The concentration of the reactant is consequently uniform in the electrolyte bulk and decreases linearly from the edge of the stagnant layer, which is also called Nernst diffussion layer, to the electrode. Theory for the hydrodynamics at the rotating disk electrode assumes that the electrode is uniformly accessible and affords a precise and reproducible control of the convection and diffusion of reactant to the electrode.

The theoretical treatment yields the concentration profile of reactant towards the RDE and defines a layer with thickness δ where diffusion is the sole mode of mass transport:

$$\delta = [\, 1.61\, \upsilon^{1/6} D^{1/3}] \, \omega^{-1/2}$$

where ω is the rotation speed ($rad.s^{-1}$), υ is the kinematic viscosity ($m^2.s^{-1}$), D is diffusion coefficient of the reacting species in the liquid ($m^2.s^{-1}$).

It can be seen that δ can be controlled by the rotation speed. From the concentration profile is derived an expression for the limiting current I_L, know as the Levich equation:

$$I_L = 0{,}62\, nFD^{0{,}67}\, \upsilon^{-0{,}166}\, cw^{0{,}5}$$

where c is concentration of reacting species ($mol.m^{-3}$), n is number of transferred electrons.

Classically, the limiting current is reached by recording a linear sweep voltammogram at a low scan rate (1-10 mVs^{-1}). At high overpotentials, the reaction kinetics is very fast and the reaction is limited by the diffusion of the reactant through the Nerst diffusion layer. The current reaches a limit I_L that increases with the rotation speed, which controls the thickness of δ.

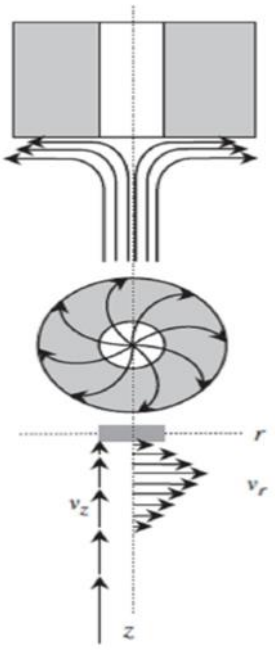

Figure 3.6. Streamlines for flow and vector representation of fluid velocities near a rotating disc electrode.

For an irreversible redox process such as the reduction of oxygen, the measured current I can be expressed as a contribution of the kinetic current I_K and the limiting current I_L, as shown in the Koutecky-Levich equation:

$$\frac{1}{I} = \frac{1}{I_k} + \frac{1}{0.201FAD_0^{2/3}\nu^{-1/6}C_0\omega^{1/2}}$$

The kinetic current is extracted from equation and given by:

$$I_K = \frac{I \times I_L}{I_L - I}$$

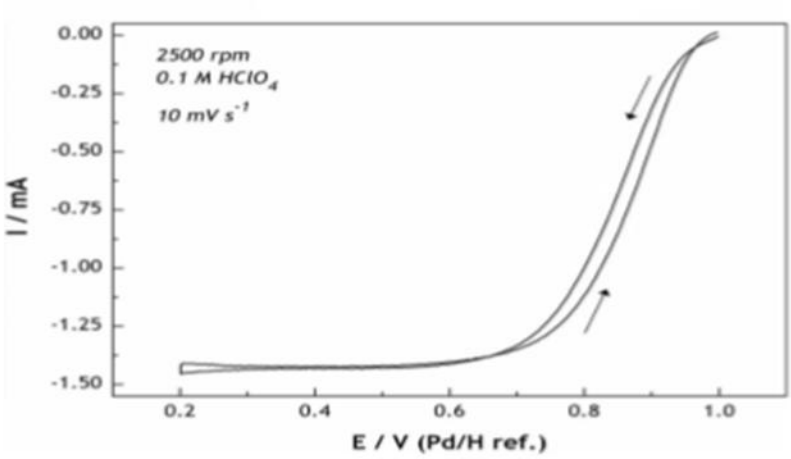

Figure 3.7. Typical rotating disk voltammogram.

3.3.2.1. Set up. The electrochemical measurements were performed in a standart three electrode cell using a Pine disc electrode as the working electrode. The electrode was made of a glassy carbon disk embedded in Teflon. Pine Instrument Company, Bipotantiostat model AFCBP1 was used. The experiment run in 0.5 M H_2SO_4 and O_2 atmosphere. The reference electrode used was Ag/AgCl. This electrode was choosen due to having better resistance than standart hydrogen electrode (SHE). End of the experiment required calculations were performed. A Pt coil served as the counter electrode (Figure 3.8).

3.3.2.2. Experimental. For electrode preparation, 0.196 cm^2 disk-electrodes were prepared by brush-coating an aqueous based catalyst ink. To prepare catalyst ink, 0.40 mg synthesized catalyst and 0.26 mL deionized water, 0.79 mL isopropyl alcohol and 0.015 mL 7% Nafion solution were used.

For experimental procedure, the cell was purged with nitrogen or argon prior to the introduction of the working electrode. The electrode was cycled in 0.5 M H_2SO_4 between -280 - 1200 mV at 10 mV s^{-1} and 1600 rpm for 30 minutes under O_2 atmosphere.

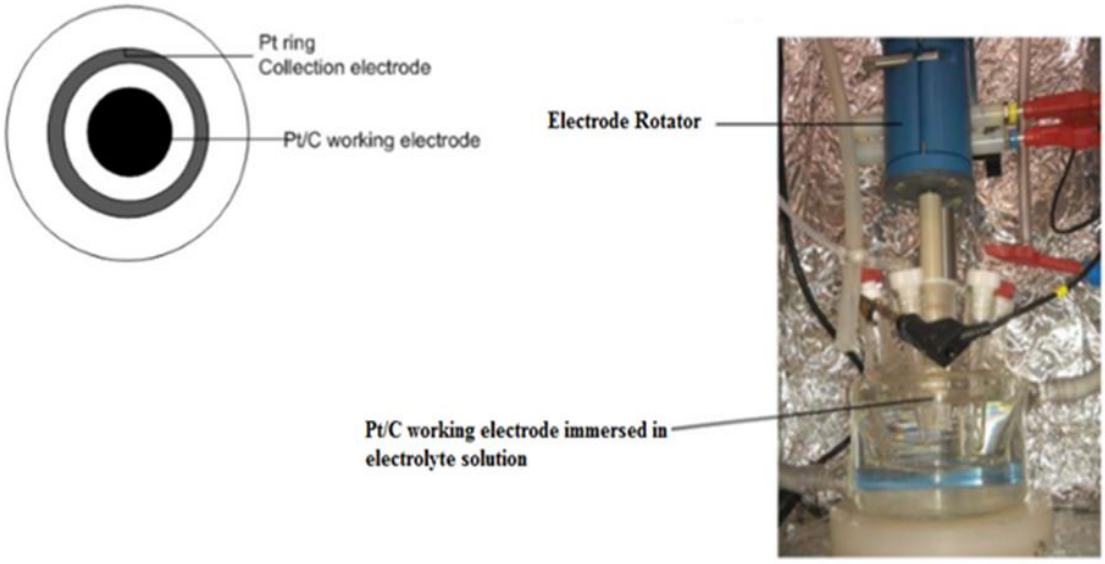

Figure 3.8. A pratical RDE setup as part of an electrochemical half-cell.

3.3.3. Performance Test

The experimental results are presented in the form of polarization curves, which show the effects of the various operating parameters on the performance of the PEM fuel cell. The performances should be measured under similar conditions.

3.3.3.1. Polarization Curve. The polarization curve is the most common electrochemical method of representing the performance of a fuel cell. It shows cell voltage against current density. Power density curve can be obtained by multiplying voltage and current density. Figure 3.9 shows a polarization curve.

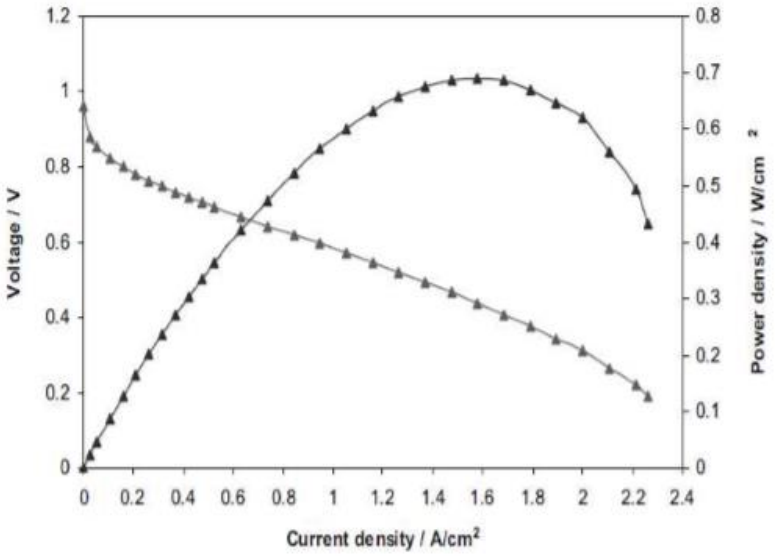

Figure 3.9. Polarization curve.

3.4. Techniques For Physical Characterization

3.4.1. Transmission Electron Microscopy (TEM)

The TEM has high spatial resolution that allowing the investigation of features of atomic size. The main use of TEM technique is to examine catalyst particle size, localized atomic structure, composition and interaction with the support.

The scheme of a typical TEM microscope is shown in Figure 3.10.

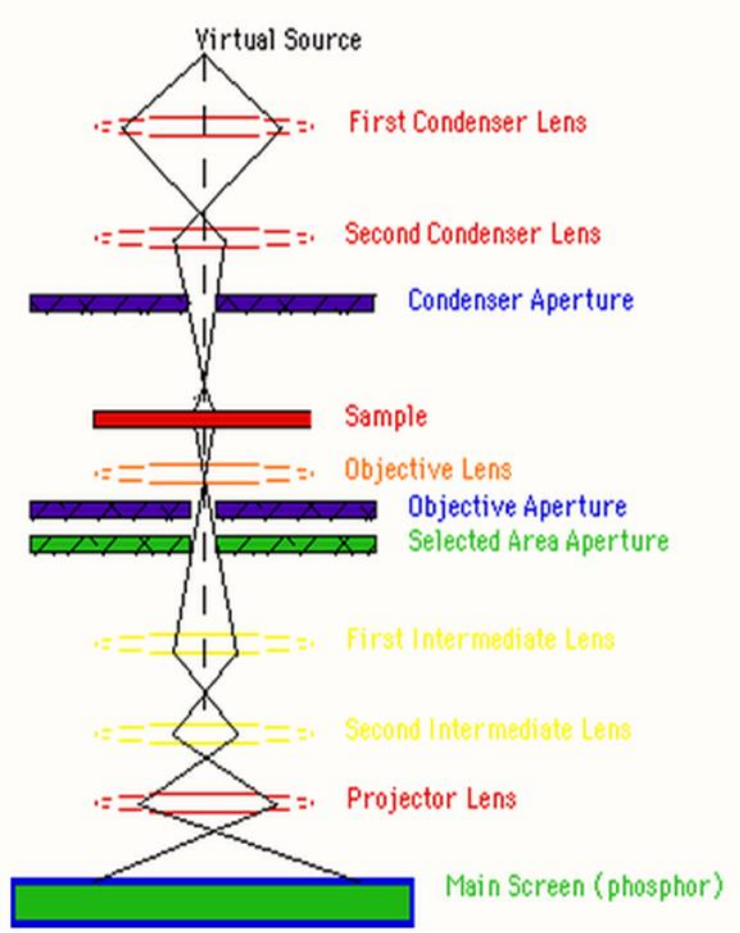

Figure 3.10. TEM microscope.

A typical TEM working as follows:

- At the top "Virtual Source" shows the electron gun, producing a flow of monochromatic electrons.

- This flow is focused to a small, thin, coherent beam by the use of first and second condenser lenses. The first lens (generally controlled by the "spot size knob") usually determines the "spot size"; the general size range of the final spot that crashes the sample. The second lens (usually controlled by the "intensity or brightness knob") actually changes the size of the spot on the sample; changing it from a wide spread spot to a pinpoint beam.

- The beam is restricted by the condenser aperture (usually user selectable), knocking out high angle electrons (those far from the optic axis, the dotted line down the center). The beam crashes the sample and parts of it which are delivered.

- The beam crashes the sample and parts of it which are delivered.

- This delivered portion is focused by the objective lens into an image.

- Optional objective and selected area metal apertures can prevent the beam; the objective aperture increasing contrast by restricting out high-angle diffracted electrons, the selected area aperture providing the user to examine the periodic diffraction of electrons by ordered adjustments of atoms in the sample.

- The image is passed down the column through the intermediate and projector lenses, being extended all the way.

- The image crashes the phosphor image screen and light is generated, allowing the user to see the image. The darker areas of the image show those areas of the sample that fewer electrons were delivered through (they are thicker or denser). The lighter areas of the image show those areas of the sample that more electrons were delivered through (they are thinner or less dense).

An electron beam is accelerated by 100-400 kV to obtain a wavelength of the order of 10^{-3} to 10^{-2} nm. The beam is oriented through a thin sample under high vacuum. When beam strikes the fluorescent screen placed at the end of the column, these emitted electrons generate the sample image. The electron beam focused and enlarged by electromagnetic lenses.

There are several parameters, which affect the resolution of the image, such as:

- The size of the objective aperture,
- The accelerating voltage applied to electrons,
- Aberrations (chromatic and spherical),
- Astigmation of the beam.

3.4.1.1. Instrumentation and experimental procedure. The TEM analyses were carried out by TUBITAK with using JEOL JEM 100C TEM device.

3.4.2. X-Ray Diffraction (XRD)

The primary use of XRD in this work is to define metallic phases in the catalysts by comparison of their diffraction patterns with known standards. It involves the identification of crystal structure of metals and determination of the average crystallite size of the metal particles.

The technique of XRD application is limited because of the restricted crystallinity of most supported metal catalyst systems. Another limitation is that only large particles can be analyzed due to severe X-Ray line broadening in case of small particles. However, where the catalyst show a degree of crystallinity and where the phases under investigation are present in adequate quantities, it is possible to have structural information, such as phase composition and crystallite size from a XRD pattern.

X-rays are electromagnetic radiations of wavelength ~1Å and they occur in electromagnetic part of spectrum between ɣ-rays and ultraviolet.

When a crystal is bombarded with X-rays of fixed wavelength and at certain incident angles, intesive reflected X-rays are produced when the wavelengths of emitted X-rays interfere constructively. When this constructive interference occurs, a diffracted beam of X-rays will leave the crystal at an angle equal to that of incident beam.

To represent this feature, consider a crystal with crystal lattice planar distance d as shown in Figure 3.11. When the travel path length difference between the ray paths 1 and 2 is an integer multiple of the wavelength, constructive interference will occur for a combination of that specific wavelength, crystal lattice planar spacing and angle of incidence θ. Each rational plane of atoms in crystal will be exposed to refraction at a single unique angle.

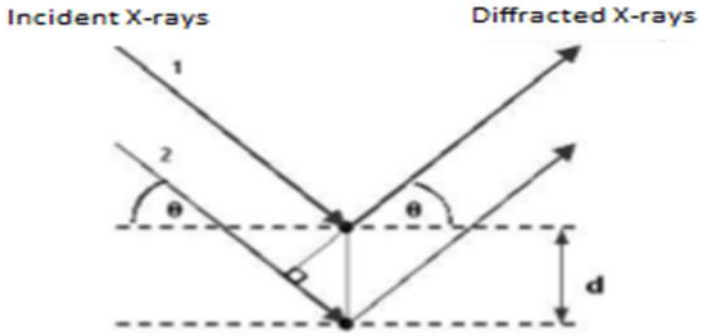

Figure 3.11. Bragg's Law reflection geometry.

The general relationship between the wavelength of the incident X-rays, angle of incidence and spacing between the crystal lattice pattern of atoms is known as Bragg's Law which is expressed as:

$$n.\lambda=2.d.\sin\theta$$

where λ is wavelength of the X-rays, d is distance between two lattice planes, θ is angle between the incoming X-rays and the normal to the reflecting lattice plane, n is integer called the order of the reflection.

Several X-ray diffraction methods for crystal size determination are available. These include Scherrer method and Rietveld refinement.

The Debye-Scherrer method corrects only for the peak broadening effect observed for sub-micrometre particles. This is achieved by the use of a shape factor K for the determination of the average crystalline size in the Debye-Scherrer formula:

$$\langle L\rangle = \frac{K\lambda}{\beta\cos\theta}$$

where L is measure of the dimension of the partice in the direction perpendicular to the reflecting plane, β is full width at half maximum of the peak (radians) corrected for instrumental broadening, K is constant that depends on the crystallite shape and is comprised between 0.9 and 1.

The Debye-Scherrer equation can only be applied to the diffraction peaks individually, which may lead to some inaccuracy in the calculation of the crystal size.

However, the Rietveld method uses structure data for the calculation of a full diffraction pattern and compares this with measured data. It also corrects for the instrument effects such as optics effects. By least squares fitting, the algorithm calculates (by varying different parameters such as peak shape or lattice constants) the minimum difference between calculated and measured patterns. Small crystallite sizes below 1μm show a peak broadening in the diffraction pattern, which results in different profile parameters. These are then used to calculate the crystallite size and the lattice parameter based on the assumption of a Gaussian size distribution.

3.4.2.1. Instrumentation and experimental procedure. The measurements were performed at Boğaziçi University Advanced Technology Research and Development Center with using Rigaku D/Max-Ultima+/PC XRD device.

3.4.3. X-Ray Photoelectron Spectroscopy (XPS)

XPS, which is also called electron spectroscopy for chemical analysis, ESCA, can give information such as the elemental composition and the oxidation state of the surface region.

Surface analysis is performed by irradiating the sample with short wavelengths from Mg Kα (1253,6 eV) or Al Kα (1486,3 eV) X-ray sources. As the photons have restricted penetrating power, they are involved in an interaction only with atoms in the surface region, which makes XPS a surface sensitive technique.

The energy of photon absorption $h\nu$ by an atom stimulates the emission of electrons with the following two processes: the photoelectric effect and the Auger process (Figure 3.11). The incoming photon ejects binding energy of a photoelectron E_b from its atomic orbital. The kinetic energy E_k of the ejected photoelectron is given by:

$$E_k = E_b - h\nu - \varphi$$

where v is the frequency of the exciting radiation, E_b is the binding energy of the photoelectron with respect to the Fermi level of the sample and φ is the work function of the spectrometer. As the gap is filled from a higher orbital, an Auger electron carries away the energy which equal to the difference in the orbitals.

The resulting spectrum is a plot of the number of electrons versus electron binding energy over a small fixed energy interval. Slight differences in orbital energies in different compounds give an enhancement to a chemical shift in the peak position and a change in the peak shape, to let differentiation of chemical species. The peak areas can be used to specify the composition of the material's surface.

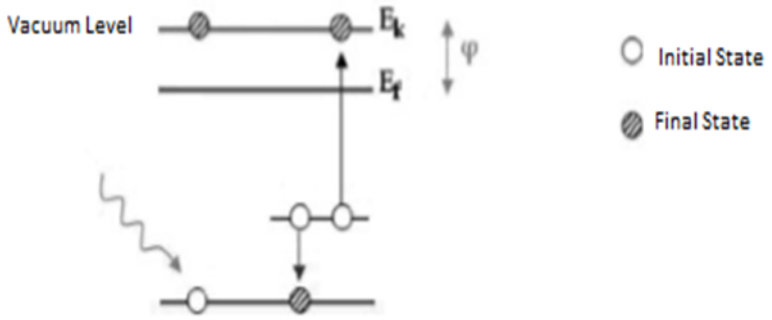

Figure 3.12. XPS emission processes for a model atom.

3.4.3.1. Instrumentation and experimental procedure. The XPS analyses were performed at Boğaziçi University Advanced Technology Research and Development Center with using Thermo Scientific K-Alpha X-ray Photoelectron Spectrometer.

4. RESULT & DISCUSSION

4.1. Cyclic Voltammetry (CV)

Cyclic voltammetry is a very useful tool for surface characterization. A cyclic voltammogram is obtained by measuring the current at the working electrode during the potential scans. The cyclic voltammetry is characterized by several important parameters; (1) the cathodic, (2) and anodic peak potantials, (3) the anodic and (4) cathodic peak currents and the half-wave potentials [53]. When the potential is ramped to the upper limit, oxidation process occur at the electrode. When the potential is reversed to the lower limit, reduction process occur at the electrode. In acidic aqueous electrolyte, noble metals absorb hydrogen and oxygen by charge transfer. However, the shape and the potential of the corresponding features are characteristic of the metal. In these experiments, cyclic voltammetry results are quite important to understand the existance of platinum electrocatalysts.

4.1.1. CV Results of Acid Treated Ni@Pt/C Nanoparticles in Acidic Environment

Cyclic Voltammetry was run in 0.5 M H_2SO_4 and N_2 atmosphere. Glassy carbon electrode was coated with prepared catalyst ink and the experiment cycled between -280 - 1200 mV at 100 mV s^{-1} . Ag/AgCl electrode used instead of standart hydrogen electrode as a reference electrode and required calculations were performed.

There are two CV results of Ni@Pt/C nanoparticles. One of them is before the acid treatment and other one is after acid treatment. After the acid treatment, it is expected to see improved CV results due to washing. It can be said that a little improvement occurred after acid treatment as is seen from the Figure 4.1 and Figure 4.2.

Characteristic H oxidation and adsorption peaks are available both CV results which means that Platinum nanoparticles exist in the solution. However, the reasons of the improvement after the acid treatment is only platinum nanoparticles exist on the shell. At

first both nickel and platinum nanoparticles are on the shell. With the acid treatment nickel nanoparticles were removed from the shell.

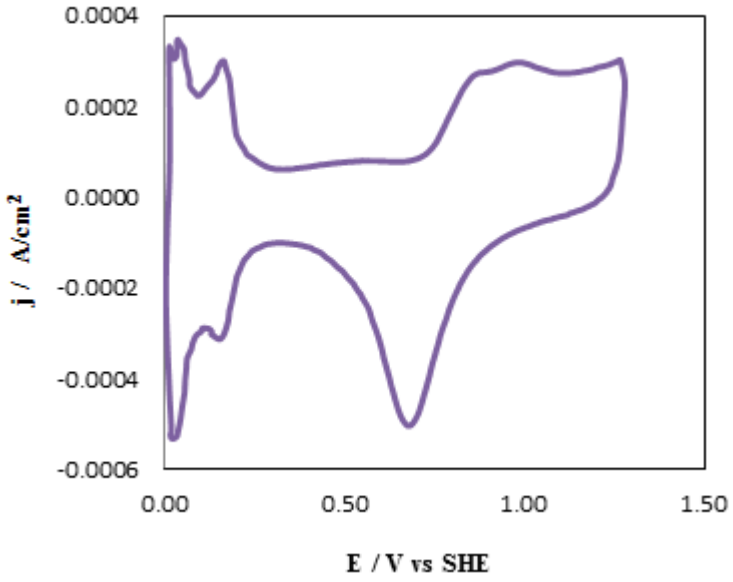

Figure 4.1. CV result before acid treated Ni-Pt.

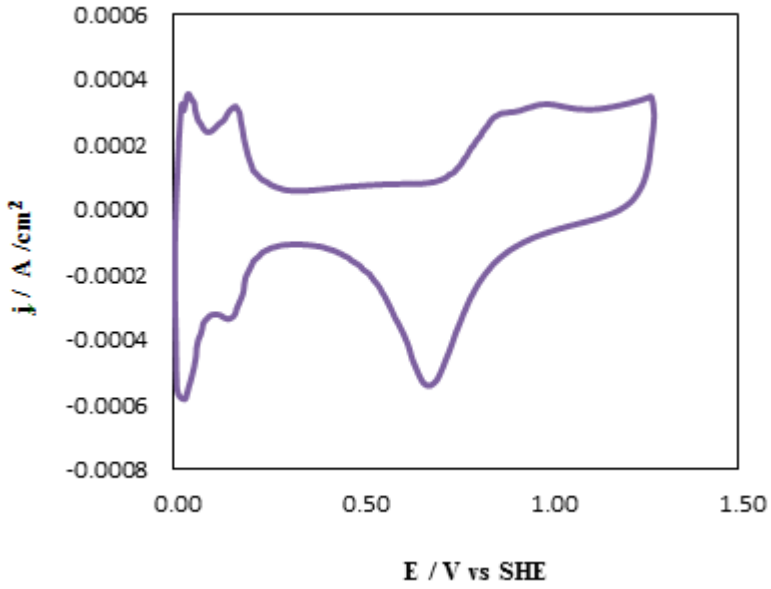

Figure 4.2. CV result after acid treated Ni-Pt.

4.1.2. CV Result of Acid Treated Ni@Pt/C Nanoparticles in Basic Environment

Cyclic Voltammetry was run in 0.5 M KOH and N_2 atmosphere. Glassy carbon electrode was coated with prepared catalyst ink and the experiment cycled between -280 - 1200 mV at 100 mV s^{-1}. Ag/AgCl electrode used instead of standart hydrogen electrode as a reference electrode and required calculations were performed.

In the experiment, KOH is used instead of H_2SO_4 electrolyte to understand the existance of nickel particles on the shell [54]. Basic environment Ni@Pt/C cyclic voltammetry result is indicated in Figure 4.3.

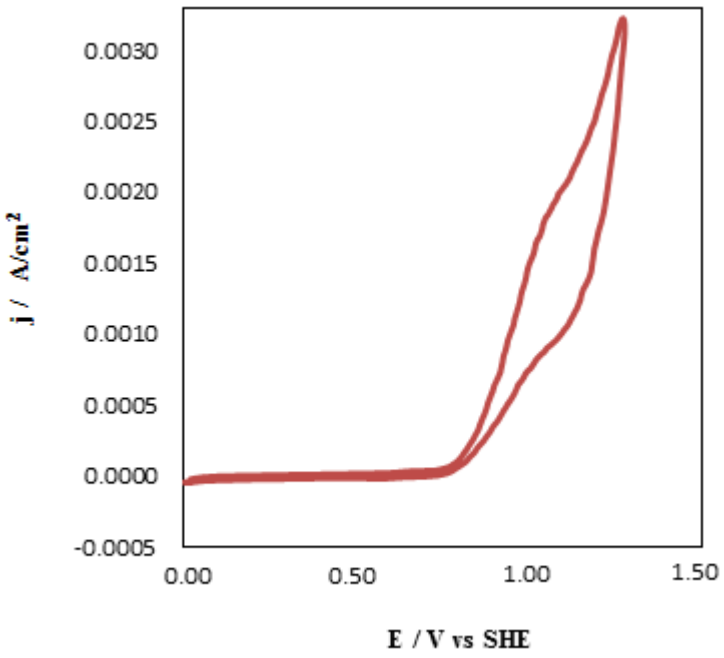

Figure 4.3. Basic environment CV result of Ni@Pt/C.

The experiment was performed to understand the existance of nickel atoms on the shell. Nickel oxidation and reduction peaks are between 0 - 0.5 V. It is clearly seen that there is no peaks, which belongs to nickel nanoparticles. Therefore, it can be said that there

is no nickel nanoparticles on the shell; they are removed from the solution with the acid treatment.

4.1.3. CV Result of Deposited Pt on Ni Nanoparticles in Acidic Environment

Cyclic Voltammetry was run in 0.5 M H_2SO_4 and N_2 atmosphere. Glassy carbon electrode was coated with prepared catalyst ink and the experiment cycled between -280 - 1200 mV at 100 mV s^{-1}. Ag/AgCl electrode used instead of standart hydrogen electrode as a reference electrode and required calculations were performed.

CV is performed to resolve whether platinum is deposited on the nickel nanoparticles. The CV result of deposited platinum on nickel nanoparticles is shown in Figure 4.4.

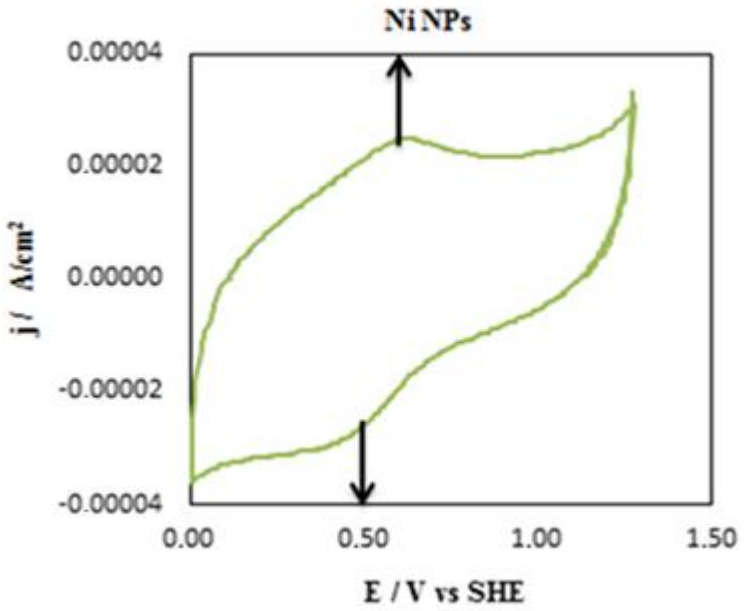

Figure 4.4. Deposited Pt on Ni nanoparticles CV result.

H oxidation or adsorption peaks, which are arising from platinum presence, cannot be seen in this scan. The small peaks exist due to nickel nanoparticles. Therefore, it can be

said that platinum did not form a shell over nickel nanoparticles. Platinum in the solution was removed as H_2PtCl_6 while washing with deionized water. Therefore, nickel - platinum core-shell structure was not formed.

4.1.4. CV Result of Deposited Pt on Co Nanoparticles in Acidic Environment

Cyclic Voltammetry was run in 0.5 M H_2SO_4 and N_2 atmosphere. Glassy carbon electrode was coated with prepared catalyst ink and the experiment cycled between -280 - 1200 mV at 100 mV s^{-1}. Ag/AgCl electrode used instead of standart hydrogen electrode as a reference electrode and required calculations were performed.

CV is performed to elucidate whether or not platinum is deposited on the cobalt nanoparticles. The CV result of deposited platinum on cobalt nanoparticles is indicated in Figure 4.5.

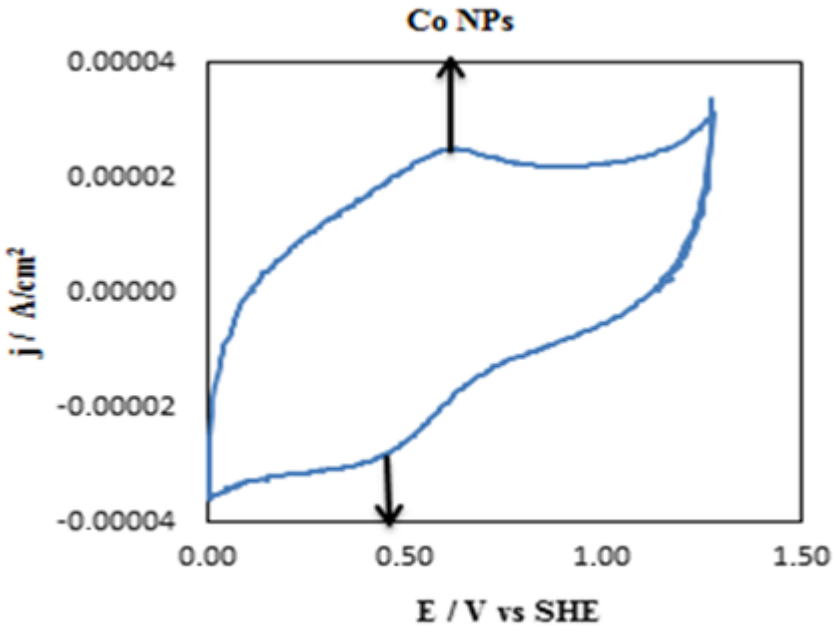

Figure 4.5. Deposited Pt on Co nanoparticles CV result.

It cannot be detected H oxidation or adsorption peaks, which are arising from platinum existance. However, the small peaks exist due to cobalt nanoparticles. Thus, platinum did not deposit on cobalt nanoparticles in the solution, platinum might be removed from the solution as H_2PtCl_6 while washed by the deionized water. There is no formation of core-shell structure.

4.1.5. CV Result of Deposited Pt on Cu Nanoparticles in Acidic Environment

Cyclic Voltammetry was run in 0.5 M H_2SO_4 and N_2 atmosphere. Glassy carbon electrode was coated with prepared catalyst ink and the experiment cycled between -280 - 1200 mV at 100 mV s^{-1}. Ag/AgCl electrode used instead of standart hydrogen electrode as a reference electrode and required calculations were performed.

CV is performed to illuminate the existence of platinum shell on the copper nanoparticles. The CV result of deposited platinum on copper nanoparticles is shown in Figure 4.6.

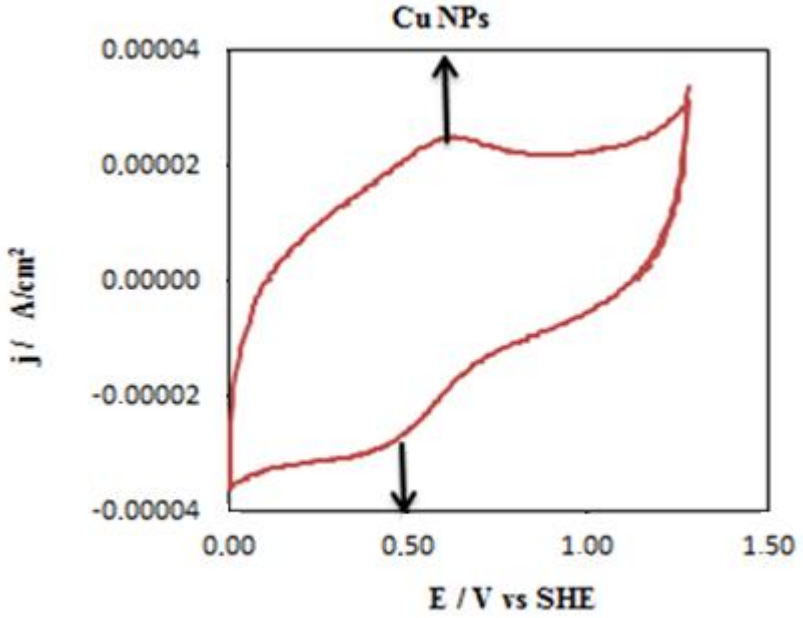

Figure 4.6. Deposited Pt on Cu nanoparticles CV result.

H oxidation or adsorption peaks, which are arising from platinum availability cannot be seen in this scan. The small peaks exist due to copper nanoparticles. Platinum did not interact with copper nanoparticles and they might be removed from the solution while washed by deionized water. Therefore, platinum did not form a shell over copper nanoparticles.

As a conclusion, cyclic voltammetry results are quite important to understand the existence of platinum electrocatalysts. Deposited platinum on metals, which are Ni, Co, Cu in this study did not give the expected outcomes. There is no H oxidation and adsorption peaks therefore it can be said that platinum nanoparticles did not exist over the transition metal nanoparticles (Ni,Cu, and Co) and there might be no interaction between platinum and transition metals. There might be several reasons; one of them is surfactant material. In the experiment of deposited platinum on nickel nanoparticles surfactant material is oleic acid. Coated oleic acid molecules can reduce the interactions between the nanoparticles [55]. Thus, oleic acid should not be used as a surfactant for this experiment. In the experiment of deposited platinum on cobalt and copper nanoparticles surfactant material is Poly-vinyl pyrrolidone (PVP). Instead of PVP, polyvinyl alcohol (PVA), polyethylene glycol (PEG) can be used [56]. However, pH conditions are quite important especially for cobalt and copper nanoparticles. If desirable pH cannot be arranged, different types of byproducts are formed in the solution and they might prevent the interaction of transition metals nanoparticles and platinum [57].

Acid treated Ni@Pt/C nanoparticles give the desired results. H oxidation and adsorption peaks are available and after the acid treatment there is an improvement of the H oxidation and adsorption peaks, because there are only platinum atoms on the surface of the nickel and platinum nanoparticles. Nickel nanoparticles were removed from the surface with the acid treatment. But in the core both nickel and platinum nanoparticles might be available.

4.2. Rotating Disk Electrode (RDE) Results

Rotating disk electrode is performed to understand the reaction kinetics of catalysts. The difference between RDE and CV is that working electrode is rotated very high speed.

Due to high speed of working electrode, mass transport is removed. Therefore, the limiting current is typically much higher than the peak current of a stationary electrode.

4.2.1. RDE Result of Acid treated Ni@Pt/C

The electrode was cycled in 0.5 M H_2SO_4 between -280 - 1200 mV at 10 mV s^{-1} and 1600 rpm for 30 minutes under O_2 atmosphere. Glassy carbon electrode was coated with prepared catalyst ink. Ag/AgCl electrode used instead of standart hydrogen electrode as a reference electrode and required calculations were performed.

Rotating disk electrode result of nickel core platinum shell nanoparticles, which was supported by carbon black, is shown in Figure 4.7.

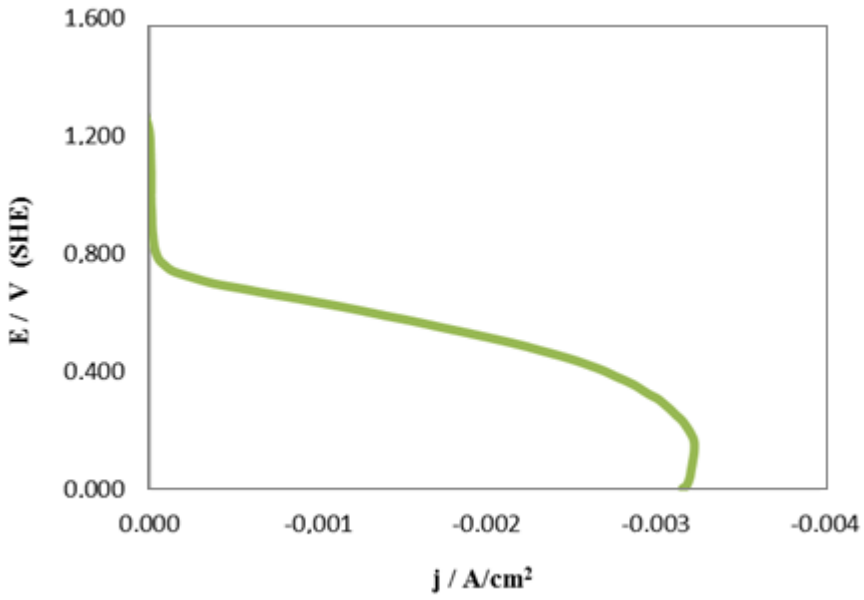

Figure 4.7. RDE result after acid treatment of Ni@Pt/C.

In Figure 4.7, current limiting value was measured as 0.0032 A/cm^2. When current equal to zero, potantial was measured as 0.88 V and this value is known as Open Circuit Voltage (OCV) [58].

4.3. X-Ray Diffraction (XRD) Results

The primary use of XRD in this work is to identify crystal structure of metals and determine the average crystallite size of the metal particles. The technique of XRD application is limited because of the restricted crystallinity of most supported metal catalyst systems. Another limitation is that only comparatively large particles can be analyzed [59].

4.3.1. XRD Result of Acid Treated Ni@Pt/C Nanoparticles

The XRD results of acid treated Ni@Pt/C compound is shown in Figure 4.8.

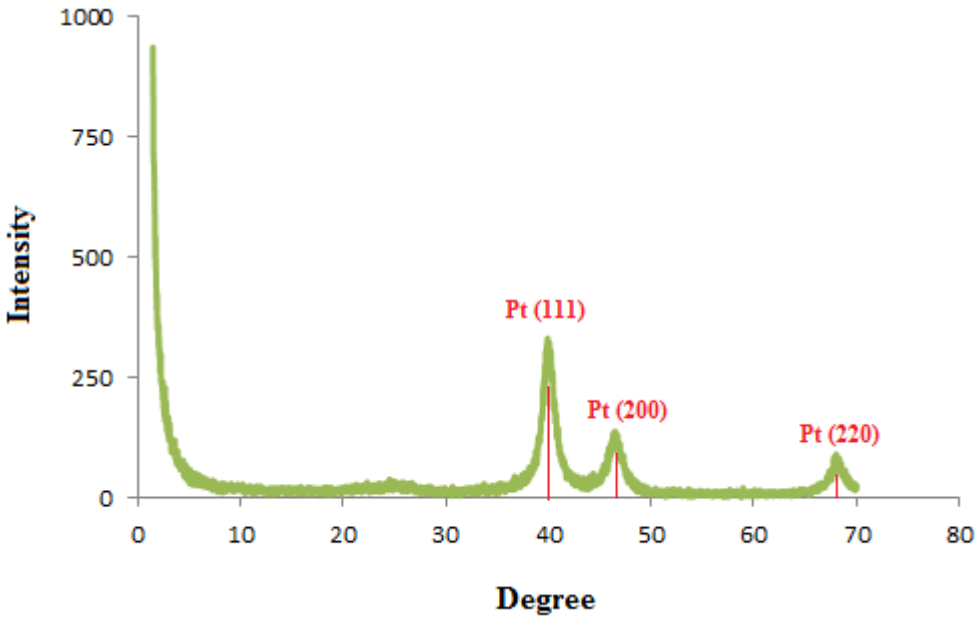

Figure 4.8. Acid treated Ni@Pt/C XRD pattern.

The characteristic (111), (200), (220) and (311) peaks for Pt (2θ =39.5, 45.9, 67.06) corresponds to face-centered cubic (fcc) Pt. It can be clearly seen that 40.1, 46.7 and 68.3 2θ peaks indicates Pt (111), Pt (200), Pt (220) respectively. When it is compared to standart fcc of Pt phase, it is obviously said that XRD patterns are completely shifted toward the higher angles. It reflects the decrease of lattice constant. This may result from

the distortion of Pt lattice due to the nickel atoms. However, a broad reflection peak at 2θ=24.6 observed due to the carbon support. It is found that there is no diffraction peak of nickel is detected in the Ni@Pt/C catalyst.

4.3.2. XRD Result of Deposited Pt on Ni Nanoparticles

The XRD results of deposited Pt on Ni nanoparticles are shown in Figure 4.9.

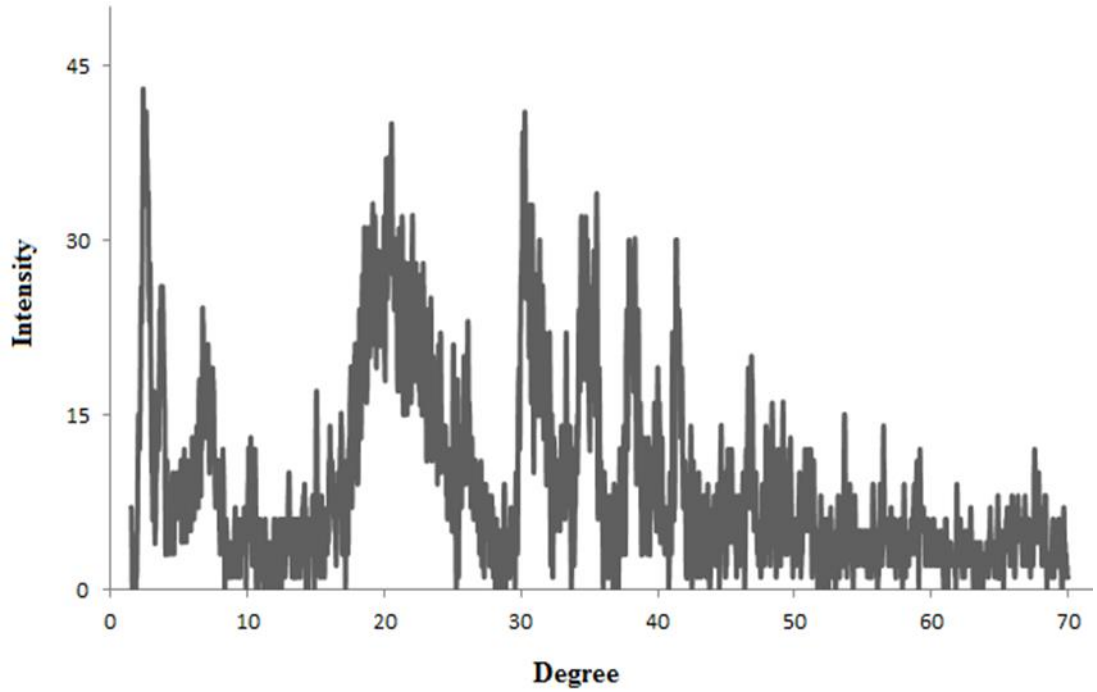

Figure 4.9. Deposited Pt on Ni nanoparticles XRD pattern.

The characteristic Pt peaks (111), (200), (220) and (311) peaks (2θ =39.5, 45.9, 67.06, and 80.7) corresponds to face-centered cubic (fcc) Pt. While the diffraction peaks at 44.5, 51.8, and 76.4 are characteristic peaks of Ni fcc structure. In Figure 4.9, the peak broadening is due to decreasing particle size. These peaks are broadened when compared to Pt metal. The results prove nanosized structure therefore a noisy xrd results are displayed. However, it cannot be seen absolute matching of platinum atoms in the Figure 4.9.

4.3.3. Deposited Pt on Co Nanoparticles XRD Result

The XRD results of deposited Pt on Co nanoparticles are shown in Figure 4.10.

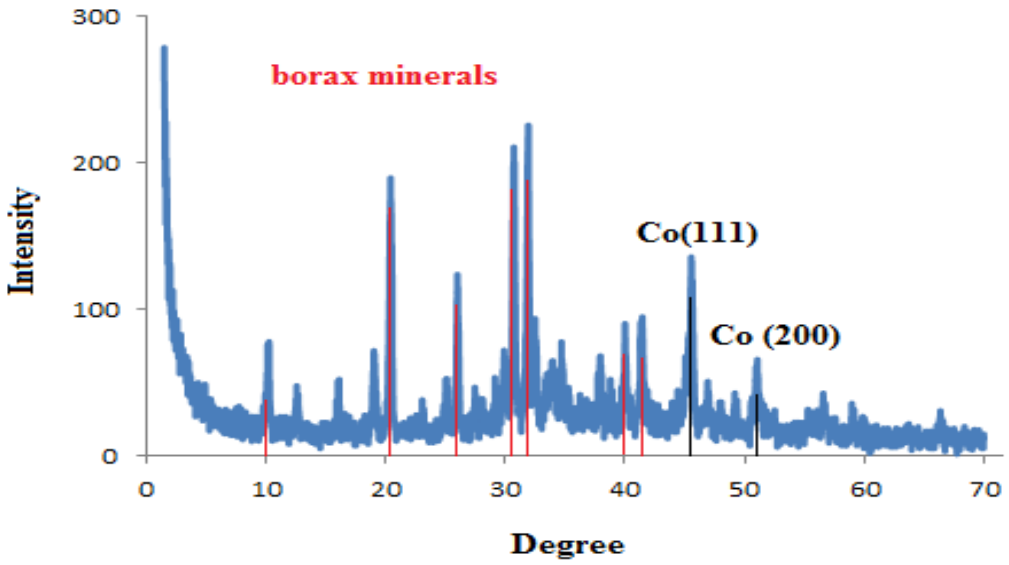

Figure 4.10. Deposited Pt on Co nanoparticles XRD pattern.

The diffraction peaks at 44, 51, and 97 are characteristic peaks of Co FCC structure. These results are summarized as amorphous structure is dominating. It cannot be seen absolute matching of platinum atoms in the Figure 4.10. It might be said that at 45, 57 and 51.05 indicates Co (111) and Co (200). However, there are some matchings of borax mineral, which comprise of sodium. To prevent forming of borax mineral, pH arrangement is required.

4.3.4. Deposited Pt on Cu Nanoparticles XRD Result

The XRD results of deposited Pt on Cu nanoparticles are shown in Figure 4.11.

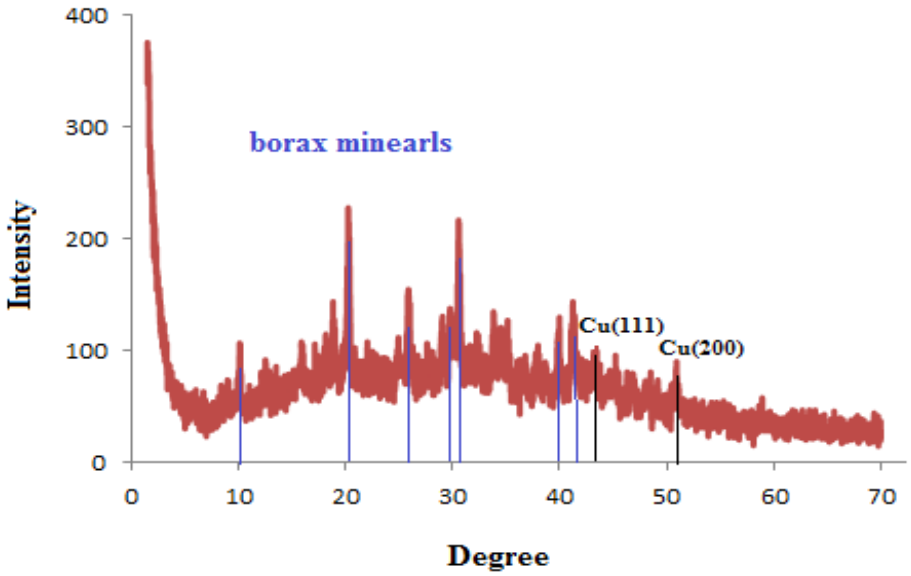

Figure 4.11. Deposited Pt on Cu Nanoparticles XRD Pattern.

The diffraction peaks at 43, 51, and 74 are characteristic peaks of Cu FCC structure. It can be clearly seen from the Figure 4.11 that amorphous structure is dominating. It cannot be seen absolute matching of platinum atoms in the Figure 4.11. It might be said that at 43.3 and 50.9 degrees indicates Cu (111) and Cu (200). Nanostructure is one of the reasons the amorphous structure. However, there are some matchings of borax mineral, which comprise of sodium. To prevent forming of borax mineral, pH arrangement is required. Especially copper and cobalt compounds are too sensitive against pH conditions.

4.4. X-Ray Photoelectron Spectroscopy (XPS) Results

XPS can give information such as the elemental composition and the oxidation state of the surface region.

4.4.1. Acid treated Ni@Pt/C XPS Result

It can be seen from the Figure 4.12 general spectrum of acid treated Ni@Pt/C XPS result.

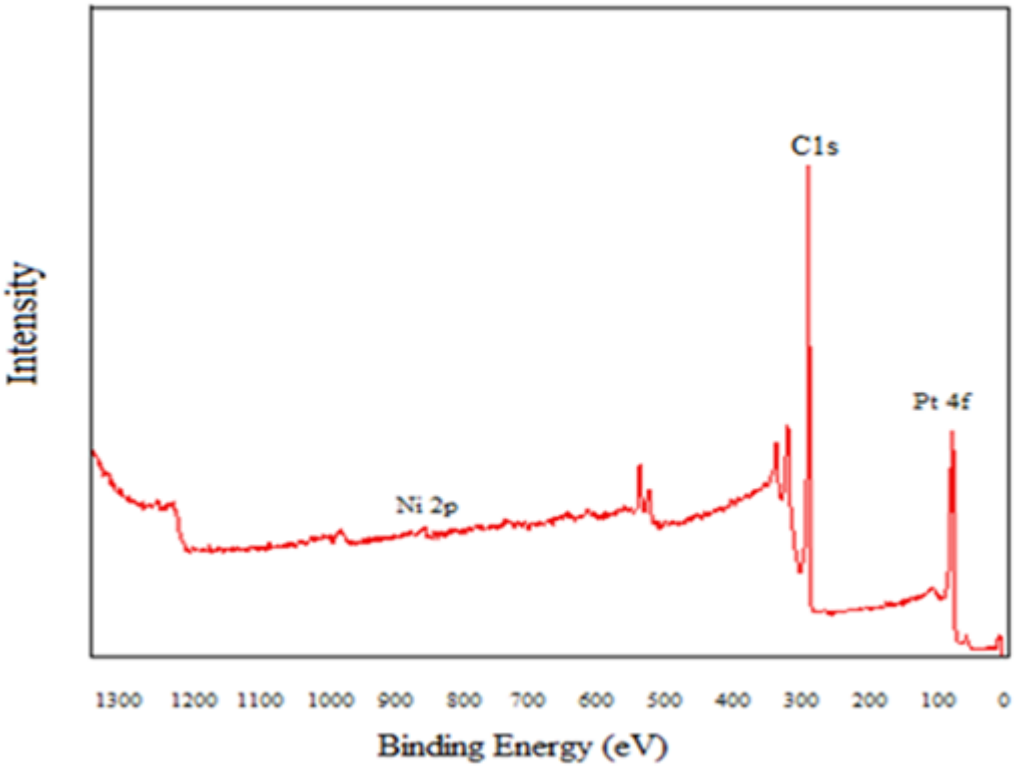

Figure 4.12. General XPS spectrum of Ni@Pt/C catalyst.

XPS is a surface sensitive technique. As is seen in the Figure 4.12 Pt specific peak is easily dedected. Carbon 1s peak also exist nearly 285eV. However, nickel specific peaks cannot be seen easily. Because with the acid treatment nickel nanoparticles removed from the surface and platinum is on the shell. Platinum existence and nickel nanoparticles removing on the surface can be proved with XPS spectrum.

In Figure 4.13 and 4.14 show the specific peaks of platinum and nickel. Nickel nanoparticles are in small quantities on the surface, which can also be seen from the specific peaks of nickel 2p.

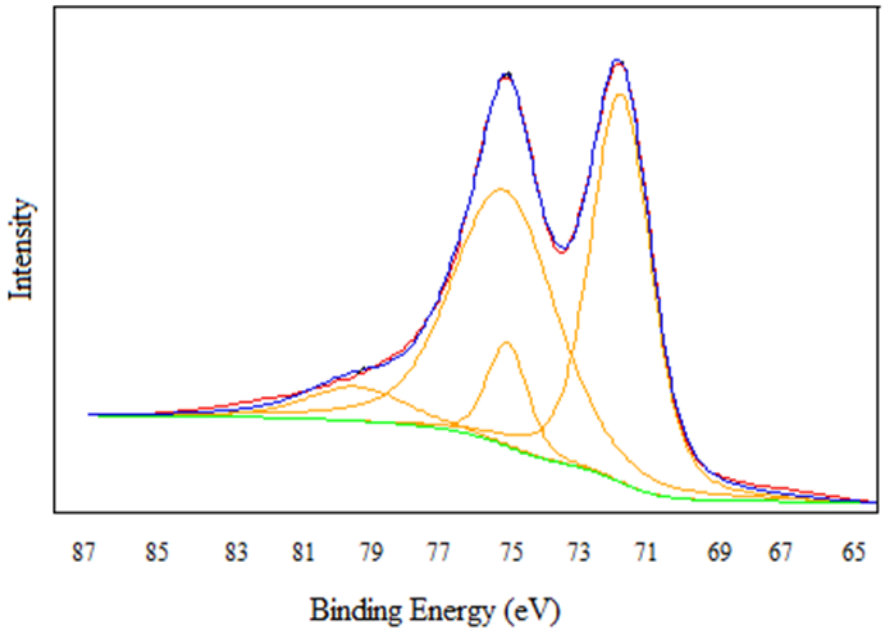

Figure 4.13. XPS spectrum of Pt 4f.

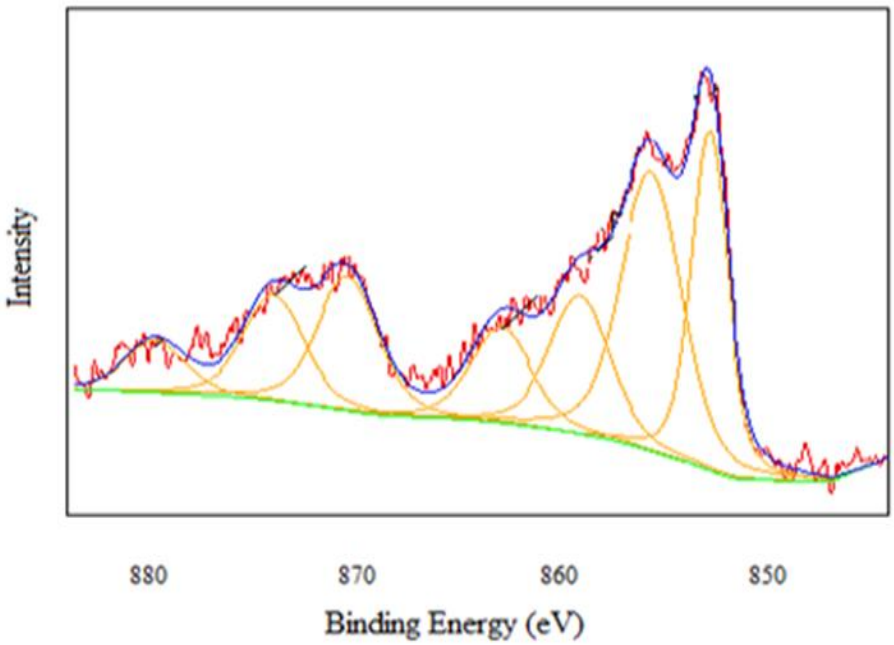

Figure 4.14. XPS spectrum of Ni 2p.

However, platinum and nickel ratios are indicated in Table 4.1.

Table 4.1. Platinum and nickel ratios in compound.

Name	Peak (BE)	FWHM (eV)	Atomic %
Pt4f Scan A	71,48	2,05	37,51
Pt4f Scan B	74,85	3,50	42,25
Pt4f Scan C	74,76	1,37	6,77
Pt4f Scan D	79,10	3,50	5,65
			Total = 92,18 %

Name	Peak (BE)	FWHM (eV)	Atomic %
Ni2p Scan A	852,77	2,09	1,56
Ni2p Scan B	855,60	3,50	2,16
Ni2p Scan C	870,34	3,50	1,06
Ni2p Scan D	862,88	3,50	0,74
Ni2p Scan E	859,07	3,50	1,07
Ni2p Scan F	873,92	3,50	0,83
Ni2p Scan G	879,65	3,50	0,40
			Total = 7,82 %

As a conclusion, XPS results show that platinum nanoparticles exist excess quantity compared to nickel nanoparticles. Platinum nanoparticles are on the surface. Nickel nanoparticles should be removed from the surface with acid treatment. XPS results prove that the surface of nanoparticles have 92% Pt and 8% Ni metals. While, only platinum nanoparticles are on the shell, both nickel nanoparticles and platinum nanoparticles should be in the core.

4.5. Transmission Electron Microscopy (TEM) Results

The main use of TEM technique is to examine catalyst particle size, localized atomic structure, composition and interaction with the support.

4.5.1. TEM Result of Acid Treated Ni@Pt/C Nanoparticles

It can be seen from the Figure 4.15 TEM results of acid treated Ni@Pt/C.

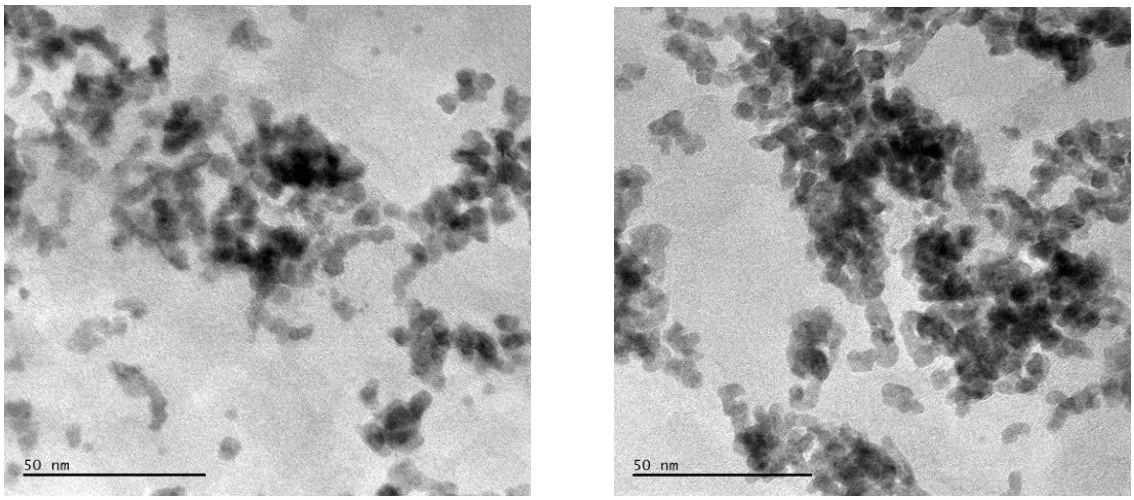

Figure 4.15. TEM images of acid treated Ni@Pt/C (50 nm).

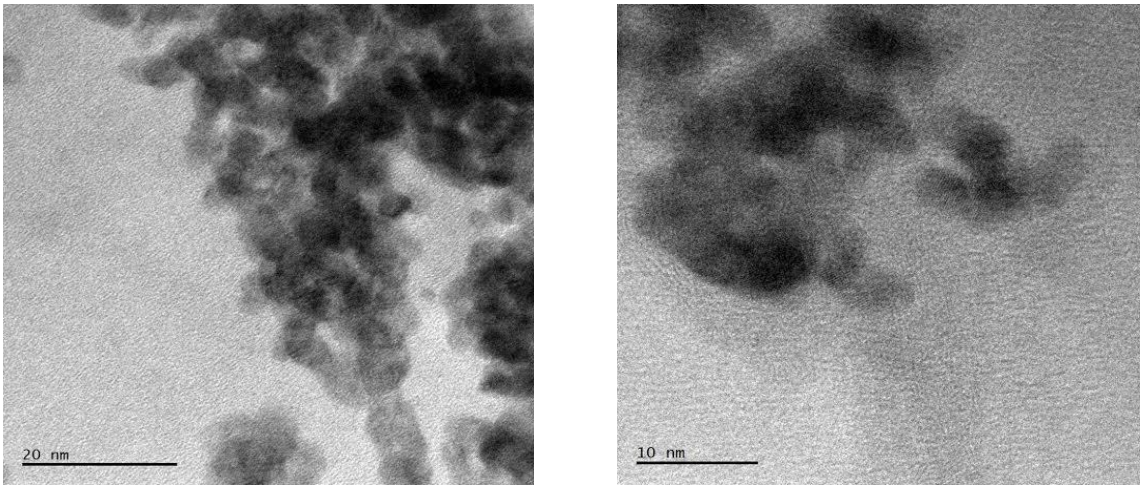

Figure 4.16. TEM images of acid treated Ni@Pt/C (20 nm-10nm).

TEM images of Ni@Pt/C catalyst were taken JEOL JEM 100C TEM microscope. Nickel-platinum core, and platinum shell nanoparticles supported by Vulcan XC-72 were well dispersed with a particle size of 4 - 5 nm.

4.6. Performance Test Result

The experimental results of performance test is presented in the form of polarization curves. The polarization curve is the most common electrochemical method of representing the performance of a fuel cell. It shows cell voltage against current density. Power density curve can be obtained by multiplying voltage and current density.

Membrane electrode assembly (MEA) was prepared as follows:

- 100 mg Ni@Pt/C catalyst and 2 mL isopropyl alcohol were sonicated for 40 minutes.
- 0.353 g Nafion (10%) was added solution and stirred over night.
- MEA was prepared and catalyst solution was sprayed on it.
- The total area of gas diffusion layer (GDL) was 25 cm^2.

Nafion 211 (25.4 μm) membrane was pretreated as follows:

- 1 hour 80^oC in 3% H_2O_2 solution,
- 1 hour 80^oC in deionized water,
- 1 hour 80^oC in 0.5 M H_2SO_4 solution,
- 1 hour 80^oC in deionized water.

After, it is boiled, oven dried and pressed. MEA thickness was measured from five different point. Average thickness was measured and appropriatete FEB gaskets were applied. MEA which had 25 cm^2 active area and gaskets were located in fuel cell test station together. After cell was connected to fuel cell test station. MEA was under N_2 atmosphere for a while and O_2 and H_2 flow were adjusted properly. Anode and cathode humidification were performed at 60^oC. While voltage was nealy 0.5 V, current draw was started to apply and MEA performance was measured at steady state.

4.6.1. Performance Test Result of Acid Treated Ni@Pt/C Nanoparticles

Open circuit voltage was measured 0.817 V at first but after 3 hours later decrease to 0.611 V. When 0.518 V was applied the system, the current level was 3.187 A. After 1 hour, it decreased to 0.068 A. It continued to work for 2 hours and there was no increasing.

There can be several reasons for this short life time and power shortage of the MEA prepared. The first reason can be the very thin Nafion electrolyte, on which pine holes can be produced when the fuel cell reactions started. Therefore, open circuit potential and performance of the fuel cell degrades very quickly due to these the gas passing thorough these pine holes. Another reason can be the excess amount of water on the cathode side, when the cell started to work under load. If the water is not drained from the cathode side, the active sides on the cathode are blocked. Hence, the performance of MEA can deteriote.

As a results of these performance test, the optimization of fuel cell peformance test is necessary. These performance test can be optimized by several parameters such as the thickness of electrolyte, air flow rate on the cathode side, the level of humidification, the operation temperature and the activation time of MEA. Since the thickness of electrolyte used is 25.4 μm, it can be increased to decrease the effect of pine holes. The flow rate and the humidification level on the cathode side, and the operation temperature of the fuel cell can be optimized very easily by controlling the OCV values. The activation period of MEA is vital for the fuel cell, since the cell and all the components of the cell is working together for the first time. Therefore, the activation period should be overnight and can be optimized by again checking the OCV values.

5. CONCLUSION

Core-shell nanoparticles were aimed to synthesize with borohyride reduction mechanism. Two different techniques were used. Synthesis of type 1 core-shell NPs, cobalt, copper, and nickel were used as a core and platinum used as a shell. First step was synthesizing core nanoparticles. After formation of core, platinum shell is attempted to place on cheap metal core. Synthesis of type 2 core-shell NPs, both core and shell synthesized together. Then, acid treatment was performed to remove the excess nickel on the surface. Hence, Nickel was in the core and platinum is on the shell. Nickel NPs were removed from the surface and only platinum NPs were on the shell. In core both nickel and platinum atoms are present.

Synthesis of type 1 core-shell NPs did not give successful results. Platinum NPs could not deposite on transition metals. Hence, shell did not form around the core. The first reason might be surfactant material. In the experiment of depositing platinum on nickel nanoparticles surfactant material was oleic acid. Coated oleic acid molecules could reduce the interactions between the nanoparticles [55]. Thus, oleic acid should not be used as a surfactant for this experiment. In the experiment of depositing platinum on cobalt and copper nanoparticles surfactant material is Poly-vinyl pyrrolidone (PVP). Instead of PVP, polyvinyl alcohol (PVA), polyethylene glycol (PEG) can be used [56]. However, pH conditions were quite important especially for cobalt and copper nanoparticles. If desirable pH could not be arranged, different types of by-products were formed in the solution and they might prevent the interaction of transition metals nanoparticles with platinum [57].

Synthesis of type 2 core-shell NPs gave desirable results. Core-shell NPs with 4-5 nm were synthesized. Both physical and electrochemical characterization techniques were performed and results showed that synthesized Ni-Pt core Pt shell catalyst material gave nearly same results with standart Pt catalysts.

The performance test of MEA prepared by Ni@Pt NPs with the particle size of 4-5 nm and the medium grade performance is observed. Therefore the optimization of fuel cell peformance test is necessary. These performance test can be optimized by several parameters such as the thickness of electrolyte, air flow rate on the cathode side, the level

of humidification, the operation temperature and the activation time of MEA. The flow rate and the humidification level on the cathode side, and the operation temperature of the fuel cell can be optimized very easily by controlling the OCV values. Therefore, the activation time can be extended overnight while checking the OCV values.

Core-shell NP formation is used to reduce the quantity of platinum. As a consequence of this effort the cost of catalysts is aimed to decrease.

REFERENCES

1. *Energy Visions,* VTT Technical Research Centre of Finland, 2009.

2. *International Energy Outlook*, U.S. Energy Information Administration, 2013.

3. *Fuel Cell Today Industry Review*, Johnson Matthey PLC, 2013.

4. *Hydrogen, Fuel Cell & Infrastructure Technologies Program, Multi-Year Research Development and Demonstration Plan*, U.S. Department of Energy, 2014

5. Giddey, S., F. T. Ciacchi and S. P. S. Badwal, "Design, Assembly and Operation of Polymer Electrolyte Membrane Fuel Cell Stacks to 1 kW_e Capacity", *Journal of Power Sources,* Vol. 125, pp. 155-165, 2004.

6. Thomas, S. and M. Zalbowitz, *Fuel Cells-Green Power,* Los Alamos National Laboratory, 1999.

7. Oster, E.A., *In Proceedings of the 16th Annual Power Sources Conference*, New Jersey, p. 22, 1962

8. Hoogers, G. and D. Thomsett, "The Role of Catalysis in Proton Exchange Membrane Fuel Cell Technology", *Cattech,* 1999.

9. Giordano, N., E. Passalacqua, L. Pinoa, A.S. Arico, V. Antonucci, M. Vivaldi and K. Kinoshita, "Analysis of Platinum Particle Size and Oxygen Reduction in Phosphoric Acid ", *Electrochimica Acta*, Vol. 36, pp. 1979-1984, 1991.

10. *Comparison of Fuel Cell Technologies*, U.S. Department of Energy, Energy Efficiency and Fuel Cell Technologies Program, 2011.

11. Marcinkoski, J., J. P. Kopasz and T. G. Benjamin, "Progress in the US DOE Fuel Cell Subprogram Efforts in Polymer Electrolyte Fuel Cells", *International Journal of Hydrogen Energy*, Vol. 33, pp. 3894-3902, 2008.

12. Holton, O. T. and J. W. Stevenson, "The Role of Platinum in Proton Exchange Membrane Fuel Cells", *Platinum Metals Review*, Vol. 54, pp. 259-271, 2013.

13. Colleen Spiegel, *Designing and Building Fuel Cells*, McGraw-Hill Professional Publishing, 1st edition, 2007.

14. Barbir, F. and T. Gomez, "Efficiency and Economics of Proton Exchange Membrane (PEM) Fuel Cells", *International Journal of Hydrogen Energy*, Vol. 21, pp. 891-901, 1996.

15. Wu, J., X. Z. Yuan, J. J. Martin, H. Wang, Jiujun Zhang, J. Shen, S. Wu and W. Merida, "A Review of PEM Fuel Cell Durability: Degradation Mechanisms and Mitigation Strategies", *Journal of Power Sources*, Vol. 184, pp. 104-119, 2008.

16. Cheng, X., Z. Shi, N. Glassa, L. Zhang, J. Zhang, D. Song, Z. Liu, H. Wang and J. Shen, "A Review of PEM Hydrogen Fuel Cell Contamination: Impacts, Mechanisms, and Mitigation", *Journal of Power Sources*, Vol. 165, pp. 739-756, 2007.

17. Wang, Y., K. S. Chen, J. Mishlera, S. C. Cho and X. C. Adroher, "A review of Polymer Electrolyte Membrane Fuel Cells: Technology, Applications, and Needs on Fundamental Research", *Applied Energy*, Vol. 88, pp. 981-1007, 2011.

18. Bose, S., T. Kuila, T. X. Nguyen, N. H. Kim, K. Lau, and J. H. Lee, "Polymer Membranes for High Temperature Proton Exchange Membrane Fuel Cell: Recent Advances and Challenges", *Progress in Polymer Science*, Vol. 36, pp. 813-843, 2011.

19. Peighambardoust, S. J., S. Rowshanzamir and M. Amjadi, "Review of the Proton Exchange Membranes for Fuel Cell Applications", *International Journal of Hydrogen Energy,* Vol. 35, pp. 9349 -9384, 2010.

20. Rikukawa, M. and K. Sanui, "Proton Conducting Polymer Electrolyte Membranes Based on Hydrocarbon Polymers", *Progress in Polymer Science,* Vol. 25, pp. 1463-1502, 2000.

21. Smitha, B., S. Sridhar and A. A. Khan, "Solid Polymer Electrolyte Membranes for Fuel Cell Applications - A Review", *Journal of Membrane Science,* Vol. 259, pp. 10–26, 2005.

22. Chandan, A., M. Hattenberger, A. El-kharouf, S. Du, A. Dhir, V. Self, B. G. Pollet, A. Ingram and W. Bujalski, "High Temperature (HT) Polymer Electrolyte Membrane Fuel Cells (PEMFC) – A Review", *Journal of Power Sources*, Vol. 231, pp. 264-278, 2013.

23. Litster, S. and G. McLean, "PEM Fuel Cell Electrodes", *Journal of Power Sources,* Vol. 130, pp. 61–76, 2004.

24. Esmaeilifar, A., S. Rowshanzamir, M. H. Eikani and E. Ghazanfari, "Synthesis Methods of Low Pt Loading Electrocatalysts for Proton Exchange Membrane Fuel Cell Systems", *Energy,* Vol. 35, pp. 3941-3957, 2010.

25. Costamagna, P. and S. Srinivasan, "Quantum Jumps in the PEMFC Science and Technology : Part I. Fundamental Scientific Aspects", *Journal of Power Sources,* Vol. 102, pp. 242-252, 2001.

26. Mehta,V. and J. S. Cooper, "Review and Analysis of PEM Fuel Cell Design and Manufacturing", *Journal of Power Sources,* Vol. 114, pp. 32-53, 2003.

27. Wee, J. H., K. Lee and S. H. Kim, "Fabrication Methods for Low Pt Loading Electrocatalysts in Proton Exchange Membrane Fuel Cell Systems", *Journal of Power Sources,* Vol. 165, pp. 667-677, 2007.

28. Zhang, L., J. Zhang, D. P. Wilkinson and H. Wang, "Progress in Preparation of Non-Noble Electrocatalysts for PEM Fuel Cell Reactions", *Journal of Power Sources,* Vol. 156, pp. 171-182, 2006.

29. Ye, S., A. K. Vijh and L. H. Dao, "Oxygen Reduction on A New Electrocatalyst Based on Highly Porous Carbonized Polyacrylonitrile Microcellular Foam with Very Low Platinum Loading", *Journal of Electroanalytical Chemistry,* Vol. 415, pp. 115-121, 1996.

30. Fournier, J., G. Faubert, J. Y. Tilquin, R. Coyte, D. Guay and J. P. Dodelet, "High Performance, Low Pt Content Catalysts for the Electroreduction of Oxygen in Polymer Electrolyte Fuel Cells", *Journal of The Electrochemical Society,* Vol. 144, pp. 145-154, 1997.

31. Kumar, G. S., M. Raja and S. Parthasarathy, "High Performance Electrodes with Very Low Platinum Loading for Polymer Electrolyte Fuel Cells", Electrochimicia Acta Vol. 40, pp. 285–290, 1995.

32. Wilson, M. S., *Membrane Catalyst Layer for Fuel Cells,* U.S. Pat. No. 5, 234, 777, 1993.

33. Cha, S. Y. and W. M. Lee, "Performance of Proton Exchange Membrane Fuel Cell Electrodes Prepared by Direct Deposition of Ultrathin Platinum on the Membrane Surface", *Journal of The Electrochemical Society,* Vol. 146, pp. 4055–4060, 1999.

34. O'Hayre, R., S. Lee, S. Cha and F. B. Prinz, "A Sharp Peak in the Performance of Sputtered Platinum Fuel Cells at Ultra Low Platinum Loading", *Journal of Power Sources,* Vol. 109, pp. 483–493, 2002.

35. Saha, M. S., A. F. Gulla, R. J. Allen, S. Mukerjee, "High Performance Polymer Electrolyte Fuel Cells with Ultra Low Pt Loading Electrodes Prepared by Dual Ion Beam Assisted Deposition", *Electrochimica Acta,* Vol. 51, pp. 4680-4692, 2006.

36. Debe, M. K., "Electrocatalyst Approaches and Challenges for Automotive Fuel Cells", *Nature*, Vol. 486, pp. 43-51, 2012.

37. Rao, C. N. R. and A. K. Cheetham, "Science and Technology of Nanomaterials: Current Status and Future Prospects", *Journal of Materials Chemistry*, Vol. 11, pp. 2887-2894, 2001.

38. Long, N. V., Y. Yang, C. M. Thi, N. V. Minh, Y. Cao and M. Nogami, "The Development of Mixture, Alloy, and Core-Shell Nanocatalysts with Nanomaterial Supports for Energy Conversion in Low Temperature Fuel Cells", *Nano Energy*, Vol. 2, pp. 636-676, 2013.

39. Norskov, J. K., J. Rossmeisl, A. Logadottir, and L. Lindqvist, "Origin of the Overpotential for Oxygen Reduction at a Fuel-Cell Cathode", *The Journal of Physical Chemistry B*, Vol. 108, pp. 17886-17892, 2004.

40. Norskov, J. K., T. Bligaard, J. Rossmeisl and C. H. Christensen, "Towards the Computational Design of Solid Catalysts", *Nature Chemistry*, Vol. 1 pp. 37-46, 2009.

41. Cramer, C. J. and D. G. Truhlar, "Density Functional Theory for Transition Metals and Transition Metal Chemistry", *Physical Chemistry Chemical Physics*, Vol. 11, pp. 10757-10816, 2009.

42. Harish, S., S. Baranton, C. Coutanceau and J. Joseph, "Microwave Assisted Polyol Method for the Preparation of Pt/C, Ru/C and PtRu/C Nanoparticles and Its Application in Electrooxidation of Methanol", *Journal of Power Sources*, Vol. 214, pp. 33-39, 2012.

43. Qi, J., L. Jiang, Q. Tanga, S. Zhu, S. Wang, B. Yia and G. Sun, "Synthesis of Graphitic Mesoporous Carbons with Different Surface Areas and Their Use in Direct Methanol Fuel Cells", *Carbon*, Vol. 50 pp. 2824-2831, 2012.

44. Chaudhuri, R. G. and and S. Paria, "Core-Shell Nanoparticles: Classes, Properties, Synthesis Mechanisms, Characterization, and Applications", *Chemical Reviews,* Vol. 112, pp. 2373-2433, 2012.

45. Wang, J. X., H. Inada, L. Wu, Y.Zhu, Y. Choi, P. Liu, W. Zhou and R. R. Adzic, "Oxygen Reduction on Well-Defined Core−Shell Nanocatalysts: Particle Size, Face, and Pt Shell Thickness Effects", *Journal of The American Chemical Society,* Vol. 131, pp. 17298-17302, 2009.

46. Kalele, S., S. W. Gosavi, J. Urban and S. K. Kulkarni, "Nanoshell Particles: Synthesis, Properties and Applications", *Current Science,* Vol. 91, pp. 1038-1052, 2006.

47. Zhang, J., M. B. Vukmirovic, Y. Xu, M. Mavrikakis and R. R. Adzic, "Controlling the Catalytic Activity of Platinum-Monolayer Electrocatalysts for Oxygen Reduction with Different Substrates", *Angewandte Chemie International Edition,* Vol. 44, pp. 2132-2135, 2005.

48. Adzic, R., J. Zhang, K. Sasaki, M. Vukmirovic, J. Wang and M. Shao, *Hydrogen Program Review,* 2006.

49. Chen, Y., F. Yang, Y. Dai, W. Wang and S. Chen, "Ni@Pt Core−Shell Nanoparticles: Synthesis, Structural and Electrochemical Properties", *The Journal of Physical Chemistry C*, Vol. 112, pp. 1645-1649, 2008.

50. Lin, R., C. Cao, T. Zhao, Z. Huang, B. Li, A.j Wieckowski and J. Ma, "Synthesis and Application of Core-Shell Co@Pt/C Electrocatalysts for Proton Exchange Membrane Fuel Cells", *Journal of Power Sources,* Vol. 223, pp. 190-198, 2013.

51. Mao, H., R. Li, K. Jiang, T. Huang and A. Yu, "Facile Preparation of Cu@Pt/rGO Hybrids and Their Electrocatalytic Activities for Methanol Oxidation", *Electrochimica Acta,* Vol. 107, pp. 419-424, 2013.

52. Wang, C., M. Chi, D. Li, D. Strmcnik, D. Vliet, G. Wang, V. Komanicky, K. Chang, A. P. Paulikas, D. Tripkovic, J. Pearson, K. L. More, N. M. Markovic, and V. R. Stamenkovic, "Design and Synthesis of Bimetallic Electrocatalyst with Multilayered Pt-Skin Surfaces", *Journal of The American Chemical Society,* Vol. 133, pp. 14396–14403, 2011.

53. Evans, D. H., K. M. O'Connell, R. A. Petersen and M. J. Kelly, "Cyclic Voltammetry", *Journal of Chemical Education*, Vol. 60, pp. 290-293, 1983.

54. Rahim, M. A. A., R.M. A. Hameed and M.W. Khalil, "Nickel as a Catalyst for the Electro-Oxidation of Methanol in Alkaline Medium", *Journal of Power Sources*, Vol. 134, pp. 160-169, 2004.

55. Zhang, L., R. He and H. Gu, "Oleic Acid Coating on the Monodisperse Magnetite Nanoparticles", *Applied Surface Science*, Vol. 253, pp. 2611–2617, 2006.

56. Liu, A. Z., J. X. Wang, C. R. He, H. Miao, Y. Zhang and W. G. Wang, "Synthesis and Characterization of Gd0.1Ce0.9O1.95 Nanopowder via an Acetic–Acrylicmethod", *Ceramics Internationa*l, Vol. 39, pp. 6229–6235, 2013.

57. Uzum, C., T. Shahwan, A. E. Eroglu, I. Lieberwirth, T. B. Scott, K. R. Hallam, "Application of Zero-Valent Iron Nanoparticles for the Removal of Aqueous Co^{2+} Ions under Various Experimental Conditions", *Chemical Engineering Journal*, Vol. 144, pp. 213–220, 2008.

58. Yuang, X. Z., C. Song, H. Wang and J. Zhang, *Springer*, Electrochemical Impedance Spectroscopy in PEM Fuel Cells, 2010.

59. Sun, S. and H. Zeng, "Size-Controlled Synthesis of Magnetite Nanoparticles", *Journal of The American Chemical Society,* Vol. 124 pp. 8204-8205, 2002.